

## Bulge-Disk Decomposition of 659 Spiral and Lenticular Galaxy Brightness Profiles

W. E. Baggett

Science Programs, Computer Sciences Corporation  
3700 San Martin Drive, Baltimore, MD 21218  
baggett@stsci.edu

S. M. Baggett

Space Telescope Science Institute  
3700 San Martin Drive, Baltimore, MD 21218  
sbaggett@stsci.edu

K. S. J. Anderson

Department of Astronomy, New Mexico State University,  
P. O. Box 30001, Dept. 4500, Las Cruces, NM 88003  
kurt@nmsu.edu

### ABSTRACT

We present one of the largest homogeneous sets of spiral and lenticular galaxy brightness profile decompositions completed to date. The 659 galaxies in our sample have been fitted with a deVaucouleurs' law for the bulge component and an inner-truncated exponential for the disk component. Of the 659 galaxies in the sample, 620 were successfully fit with the chosen fitting functions. The fits are generally well-defined, with more than 90% having RMS deviations from the observed profile of less than 0.35 magnitudes. We find no correlations of fitting quality, as measured by these RMS residuals, with either morphological type or inclination. Similarly, the estimated errors of the fitted coefficients show no significant trends with type or inclination.

These decompositions form a useful basis for the study of the light distributions of spiral and lenticular galaxies. The object base is sufficiently large that well-defined samples of galaxies can be selected from it.

*Subject headings:* galaxies: spiral — galaxies: photometry

## 1. Introduction

In order to compare the large-scale characteristics of galaxies objectively, quantitative measures of the structural components are necessary. There are many schemes for describing the structure of galaxies, including Hubble classification (Sandage, 1961), isophotal radii (Holmberg, 1947), concentration parameters (Kent, 1985; Kodaira et al., 1990), and the use of various fitting functions (deVaucouleurs, 1953; Freeman, 1970; Kormendy, 1977). All these techniques specify parameters which can provide insight into the formation and evolution of galaxies. The use of standardized fitting functions is arguably the most powerful method for measuring the large-scale structure of galaxies, as the functions yield a variety of parameters which can be easily compared with the results of theoretical models. They also provide a reasonably detailed description of the radial light distribution with a small number of parameters.

Ideally, fitting functions would be based upon the physics of the formation and evolutionary processes. Unfortunately, these processes are neither simple nor well-understood, so the most commonly used functions are derived empirically. Traditional fitting functions for elliptical galaxies and spiral galaxy bulges include the Hubble law (Hubble, 1930), King model (King, 1966), and deVaucouleurs law (deVaucouleurs, 1953). Recently, there has been some work which suggests that a generalized version of the deVaucouleurs profile ( $r^{1/n}$ ) provides for better bulge fits (Andredakis, Peletier, and Balcells, 1995), and that late-type spirals often have bulges which are best fitted by exponentials (Andredakis and Sanders, 1994). Exponentials (Freeman, 1970) and inner-truncated exponentials (Kormendy, 1977) work well for the disk components of spiral galaxies. Overall, the deVaucouleurs law seems to be quite effective as a fitting function for bulges; it can be written as

$$I_B(r) = I_e \times 10^{-3.33((r/r_e)^{1/4}-1)} \quad (1-1)$$

where  $I_B(r)$  is the surface intensity of the bulge at radius  $r$ ,  $r_e$  is a characteristic radius defined to be the radius within which half the total light is emitted, and  $I_e$ , the effective intensity, is simply the surface intensity at  $r_e$ . (In this paper, we will consistently use the term "surface intensity,"  $I$ , to mean linear intensity units per square arcsecond, and "surface brightness,"  $\mu$ , to mean the same quantity in magnitude units.) Similarly, the inner-truncated exponential is defined by Kormendy (1977) as

$$I_D(r) = I_0 \times \exp -(r/r_0 + (r_h/r)^n) \quad (1-2)$$

where  $I_D(r)$  is the disk surface intensity at radius  $r$ ,  $I_0$  is the central intensity of the disk,  $r_0$  is the disk scale length, and  $r_h$  is the radius of the central cutoff of the disk ("hole radius"); the pure exponential disk is the same as equation (1-2) with  $r_h = 0$ . Kormendy (1977) found that a value of  $n \sim 3$  in the truncation term works well, and we have adopted  $n = 3$  for all of the fits presented

here. Figure 1 illustrates the usefulness of including a truncation term in the fitting function, using NGC 3145 as an example.

Others have used these fitting functions to obtain the relevant structural parameters for spiral galaxies in order to compare galaxies of different types, luminosities, and environments. For example, Boroson (1981) fit brightness profiles for 26 non-barred spiral galaxies in order to determine how the bulge-to-disk ratios are related to the Hubble types, and to investigate the relationship between spiral and S0 (lenticular) galaxies. Kent (1985) performed a similar analysis using 105 intrinsically luminous galaxies of all types. Kormendy (1977) decomposed the brightness profiles of seven compact S0 galaxies and one "normal" galaxy to check Freeman's (1970) hypothesis of a constant central disk surface brightness. More recently, deJong (1996) investigated the Freeman (1970) result of a constant central surface brightness of disks, and some other relationships between the fitting parameters and the Hubble sequence, using  $B$ - and  $K$  - *band* brightness profiles of 86 face-on disk galaxies.

A relatively recent innovation is to fit a surface to the entire galaxy image (Byun and Freeman 1995) using the above fitting functions and also solving for the center and ellipticity of the projected distributions. A general advantage of this approach is that the bulge and disk components can be allowed to have different ellipticities, which alleviates the problem of projection effects for moderate- to high-inclination systems: because the rounder bulge is typically sampled at a smaller galactocentric radius than the inclined disk for a given position in the image, the derived bulge parameters are systematically too large when estimated from brightness profiles obtained by azimuthal averaging techniques. However, the profiles used here are major axis cuts (see below), so this difficulty should not affect our fitted parameters (Burstein 1979). The cost of using major axis cuts is that of throwing away much of the information in the images.

All of these programs except Kormendy (1977) employed a simple exponential to describe the disk light distribution. As part of a study of the origin of inner-truncated spiral galaxy disks, or Type II brightness profiles (Freeman, 1970), we have used the deVaucouleurs' law and the inner-truncated disk fitting function from Kormendy (1977) for the bulge-disk decomposition of 659 spiral and lenticular galaxy brightness profiles. Our preliminary study (Baggett, Baggett, and Anderson, 1993) indicated that a substantial fraction of all spiral galaxies exhibit an inner-truncation, so the inclusion of such a term in the fitting function seems justified with this large set of brightness profiles. Furthermore, the data set used in this study is extremely homogeneous, all images having been obtained, reduced, and analyzed in the same way. Thus, the results of our fitting should be a useful resource for many studies of the large-scale properties of disk galaxies. The following sections will describe the data and the bulge-disk decomposition procedures, and will present the fitting results together with a discussion of the associated errors.

## 2. Data

The brightness profiles used for this study were obtained from Kodaira et al. (1990; hereafter, PANBG) in a machine-readable form. The initial PANBG sample of galaxies was selected on the basis of being included in *A Revised Shapley-Ames Catalog of Bright Galaxies* (Sandage and Tammann, 1981; hereafter, RSA) and being north of declination  $-25^\circ$ . Of the 911 such galaxies in the RSA, 791 are included in the PANBG, and 659 of those have Hubble types (T-Types) from the *Third Reference Catalogue of Bright Galaxies* (deVaucouleurs et al., 1991; hereafter RC3) in the range -3 to 9, which indicates that they are spiral or lenticular galaxies. These 659 galaxies form the basis of our study.

Galaxies in the PANBG were observed photographically over a period of almost two decades (late 1970’s through 1988) with the Kiso Observatory 1.05-m Schmidt telescope, using Kodak IIa-D plates and a Schott GG495 glass filter to define the “photographic V-band.” Exposure times ranged from 30 minutes to 60 minutes, with 50 minutes being standard, and the plates were developed in Fuji Pandol or Kodak D-19 developer. The plates were then digitized with the Kiso Observatory PDS microdensitometer utilizing a  $1''$  square aperture, except for NGC 224 and NGC 598, which were measured with a  $10''$  square aperture. Each plate included a step wedge image which was scanned in the same fashion as the galaxy images. Measured densities were converted into relative intensities via the wedge calibrator, and the aperture photometry from Longo and deVaucouleurs (1983) was then used to transform the resulting magnitudes to a standard photometric system. The stated internal photometric accuracy in the PANBG is about 0.1 magnitudes (standard deviation), and is dominated by errors in the absolute calibration.

The brightness profiles in the PANBG were obtained from the resulting calibrated images by taking a cut along the apparent major axis of each galaxy. The major axis was defined by fitting the  $25 V - mag \text{ arcsec}^{-2}$  isophote with an ellipse whose center was fixed at the center of gravity of a  $21 \times 21$  pixel region around the apparent nucleus of the galaxy. The surface brightness was then sampled along this axis using a circular aperture which was stepped outward from the galaxy center in 2-pixel steps ( $2''$  for all but NGC 224 and NGC 598, which used  $20''$  steps). The aperture used was 2 pixels in diameter at the galaxy center and the diameter was varied in such a way as to be tangent to a sector with a 5 degree vertex angle centered on the major axis. This scheme of varying the aperture size was chosen in order to compensate for the decreased signal-to-noise ratio in the outer portions of the galaxies. As a result, there is some radial smearing of the intensity information at large galactocentric radii, smoothing structure in the outer portions of each profile. Further smoothing results from our averaging of the two halves of the major axis cut to produce the final profiles. For full details of the data acquisition and reduction processes, the reader is referred to PANBG.

## 3. Fitting

### 3.1. Procedure

The major axis brightness profiles were fitted using a combination of a deVaucouleurs' (1953) law (equation 1-1) and an inner-truncated exponential (Kormendy, 1977; equation 1-2). The interactive STSDAS task 'nfit1d' was used for all of the fitting; this task uses the downhill simplex algorithm for performing a non-linear least-squares fit of the data to a specified function, and allows interactive control over the inclusion of the various parameters and the range of the data to be fit. It is a very flexible routine and we found that it accurately returns the values of the fitting parameters in a number of test cases. Fitting is performed on the surface intensity data and is accomplished by minimizing the weighted RMS deviation of the data from the fit.

The most appropriate weighting function,  $w_i$ , is one which uses the variance of the intensity measurement for each point as its basis, with the weight of the  $i^{th}$  point being

$$w_i = \frac{1}{\sigma_i^2} \quad (3-1)$$

where  $\sigma_i^2$  is the variance of the  $i^{th}$  point (Bevington, 1969). We chose to use a weighting based on the Poisson distribution, where  $\sigma_i \propto \sqrt{I}$ , as this was consistent with the fashion in which the intensity measurements were obtained.

An unfortunate side effect of this  $1/I_i$  weighting function is that it destroys the usefulness of the weighted RMS residual as a goodness of fit measure *between* galaxies. The value of the weighted RMS residual is highly dependent upon the fitting range, with fits to lower surface intensities being virtually guaranteed a lower weighted RMS value than fits stopping at higher surface intensities. As a result, the weighted RMS residual is a useful diagnostic only during the fitting process for a given galaxy and, as such, the weighted RMS values for each fit are not reported here.

However, the *unweighted* RMS residuals,  $\sqrt{[\sum(\mu_i - \mu_{fit})^2]/N}$ , can be computed after the fact, and we have tabulated these values, expressed in magnitude units, as a basis for assessing the relative quality of the fits. These residuals were computed from the portions of each brightness profile at radii larger than  $3''$  and out to the point where the profile first drops to a surface brightness fainter than  $25 V - mag \text{ arcsec}^{-2}$ . Hence, all of the calculations avoid the portion of the profile most affected by seeing, and reach the same limiting surface brightness. Also, any structure present in the profile contributes to this measure, and thus galaxies with significant structure will be recognizable by their correspondingly larger RMS value. In this way, the unweighted RMS residuals are directly comparable from galaxy to galaxy, and reflect more accurately the quality of the fits than do the weighted RMS residuals.

Aside from the weighting function, the only other controlled aspect of the fitting was the choice of components to include in each fit. Generally, all fits were attempted with both a bulge and a pure exponential disk, resulting in the estimation of four quantities and their uncertainties:  $I_e$ ,  $r_e$ ,

$I_0$ , and  $r_0$ ; inner-truncated disks, with the additional parameter,  $r_h$ , were only utilized if the profile had the suggestion of a plateau near the center. If any component (bulge, disk, inner-truncated disk) was fit with a negative value for a coefficient, that component was deemed non-physical and was removed from the fitting function. In cases where the need for a specific component was not obvious, fits with and without it were obtained and the component was included if the *weighted* RMS value was smaller by at least 10% than the fit without the component.

A sample of the results of the fitting are presented in Table 1, which provides for each galaxy its NGC/IC designation (as indicated by a leading "N" or "I", respectively), its revised Hubble type, T-type, and axis ratio from the RC3, and the fit parameters determined here. The fit parameters are given as the fitting range in arcseconds (in the format minimum:maximum), the bulge effective surface brightness ( $\mu_e$ ), the bulge effective radius ( $r_e$ ), the disk central surface brightness ( $\mu_0$ ), the disk scale length ( $r_0$ ), and the disk hole radius ( $r_h$ ). The table also includes the seeing as reported in the PANBG, and the seeing-corrected values of the fitted bulge parameters ( $\mu_e^0$  and  $r_e^0$ ; see the Appendix). The last two columns contain the unweighted RMS deviation of the fit from the profile in  $V - mag \text{ arcsec}^{-2}$  and a column of notes. All surface brightness quantities are in units of  $V - mag \text{ arcsec}^{-2}$ , and all radii are in units of arcseconds. No corrections for galactic extinction, internal extinction, or inclination have been applied — the fits are for the observed major axis profile. We have chosen to present the results for the observed profiles in order to allow the reader the opportunity to apply the corrections (s)he deems most appropriate; we therefore avoid the necessity of uncorrecting our fits and subsequently applying a different correction.

The fitting procedure did not include any allowance for the effects of seeing on the brightness profile. In the Appendix, we describe an experiment which was designed to quantify the impact on the fitted bulge parameters of excluding seeing from the fitting; the net result is that our fitted  $I_e$  tends to be too large by up to an order of magnitude when the seeing is much larger than the input effective radius, and our fitted  $r_e$  tend to be slightly too small in the same cases. This is what is intuitively expected, of course.

Although the profile definition procedure introduces a significant level of radial smearing, structure is still apparent in many of the profiles. The fitting process nominally made no allowance for the presence of structure, fitting across arms and bars as if they were simply noise in the data, except in some specific instances. These instances occur when a very strong, isolated feature is present — then the radial range occupied by the feature was excluded from the fit. If a strong feature is present at the end of the fitting range, the fitting range was suitably shortened. The existence of such a condition was manually determined, and is indicated in Table 1 by the presence of multiple ranges in the fitting range column and/or by a note ("A") in the last column of the table.

Figure 2 presents the profiles and fits for the galaxies from Table 1. Each plot shows the observed profile from the PANBG as crosses, and the fitted bulge and disk components and their

sum as solid lines. In addition, the range of radius included in the fit is indicated by the horizontal line(s) at the  $25.3 V - mag \text{ arcsec}^{-2}$  level, and the fit parameters are provided near the top of each plot. This selection of objects includes some very good fits as measured by the RMS deviations (NGC 0016, NGC 0404), some typical-quality fits (NGC 0224, NGC 0237), some fits which avoid strong structure in the profile (NGC 0151, NGC 0157, NGC 0253), and one of the worst fits in the entire sample (NGC 0289).

There were 39 galaxies in the sample for which no fits were obtained; these objects are listed in Table 2, with their revised types and axis ratios from the RC3. These galaxies are particularly ill-suited for fitting by the selected fitting functions, as many of them have pronounced concavities toward low surface brightness or multiple exponential components in their brightness profiles – the chosen functions simply do not represent their light distributions in any meaningful way.

Finally, there are also several fits (e.g., NGC 0016, NGC 0628, NGC 0890, and NGC 5033) where the disk component is everywhere fainter than the bulge, and other fits where the disk becomes brighter than the bulge only at intermediate radii (e.g., NGC 0670, NGC 0955, NGC 1090, and NGC 1187). In both of these situations, the bulge fit might have benefitted from an alternative functional form, perhaps the generalized deVaucouleurs’ law as discussed by Andredakis, Peletier, and Balcells (1995), although no attempt has been made to investigate this in the present study.

### 3.2. Fitting Errors

We have chosen three methods of estimating the fitting errors: 1) unweighted RMS residuals, 2) error estimates provided by the fitting software, and 3) comparison with the results of other workers.

The unweighted RMS residuals for each fit are tabulated in Table 1. Because we have computed them in a uniform fashion for all objects, including all structure in the profiles, these values provide an unbiased and consistent measurement of how well the fitting functions and the determined parameters describe the observed brightness distribution. From these values we find that the median RMS deviation of the fits is only 0.15 mag, and that more than 90% of the fits are better than 0.35 mag; Figure 3 shows the distribution of the RMS deviations using bins of width 0.05 magnitude. The overall ability of the fits to describe the brightness distributions is quite good, given that the unweighted RMS residuals include all of the structure present in the profile.

In an effort to quantify the value of the unweighted residuals as a measure of the goodness of fit, we have examined plots of the profiles and selected the best examples of profiles without significant structure and which appear to be well represented by the chosen fitting functions. Note that this selection did not involve consideration of the computed unweighted RMS residuals. There were 16 objects included in this selection, and they have a mean unweighted RMS deviation of 0.05 magnitudes and a range of 0.03 magnitudes to 0.10 magnitudes; this suggests that fits with unweighted RMS residuals greater than about 0.10 magnitudes are affected to some degree by

significant structure and/or poor fitting quality. The full sample contains 161 galaxies with RMS residuals of 0.10 magnitudes or less.

At the other end of the distribution, the worst-fit galaxies have been investigated to attempt to find out why they were so poorly fit. We have inspected the 18 galaxies which have unweighted RMS residuals greater than 0.5 magnitudes to search for common characteristics such as morphology and inclination. The T-Type distribution of these 18 galaxies is essentially the same as for the sample as a whole, so there appears to be no correlation between poor fit and T-Type. There also appears to be no serious trend with inclination: the mean inclination of the group is  $57^\circ$ , consistent with a random distribution of tilts. The most common characteristic is a low-surface brightness extension to the brightness profile, such that the fit falls below the measurements in the outer portion. The extension is sometimes featureless, sometimes it contains a distinct bump (as if an outer ring or arm); sometimes it is nearly constant brightness and other times it is more or less parallel with the inner profile. There is only one case (NGC 0157) where the problem region is in the main portion of the disk, and this galaxy looks disturbed, almost as if undergoing a collision. The apparent overriding reason for the poor fits is simply that the chosen fitting functions do not work well for some galaxies. This same conclusion holds for the 39 galaxies which were not fitted in this effort: common characteristics of these objects are extremely strong, large-scale structures, concavity of the brightness profile toward faint surface brightness, and apparent multiple components of the profile, usually with more than one exponential. This occasional inappropriateness of the fitting functions suggests that careful consideration of the fitted parameters and their error estimates should be exercised before judging whether a specific fit is truly meaningful for a detailed study of any individual galaxy.

The second method of judging the fitting errors was the use of estimated coefficient errors as produced by the fitting software. The 'nfit1d' task estimates the errors in each parameter by a process of bootstrap resampling, with a choice of distribution functions for use in the procedure. We used the Poisson distribution as the distribution function for the parameter error estimation as this reflects the photon statistics expected to affect the measured relative intensities in the brightness profiles. In order to minimize the effects of comparing parameters which vary wildly in value from galaxy to galaxy, we have computed the fractional error in each fitted parameter. Table 3 lists these fractional error estimates for a sample of the galaxies — column 1 gives the galaxy identification and columns 2 through 6 the fractional error of each of the parameters. Note that since the fitting was performed in the surface intensity scale (not surface brightness), the relative errors are computed in linear units, not magnitude units.

The fractional errors for the full set of galaxies are summarized in Table 4, which gives for each parameter the number of error estimates, the mean fractional error, the standard deviation of the fractional errors, the median fractional error, and the minimum and maximum fractional errors. As can be seen in Table 4, every parameter *except*  $I_0$  is significantly affected by outliers; histograms of the fractional error of each parameter are shown in Figure 4, which demonstrate this problem. Removing the most discrepant outlier from the statistical calculations (second part



of Table 4) improves the results considerably. Unfortunately, there is not just one "bad" fit in the sample causing all of these outlying points: the bulge parameter errors are both dominated by the fit for NGC 2441, while the disk central surface intensity error is affected by the fit for NGC 2541, the disk scale length error by NGC 5033, and the hole radius error by NGC 2997.

The bulge component of NGC 2441 dominates the disk only at radii smaller than about 6 arcsec, so there are very few data points defining the bulge and the coefficient uncertainties reflect this fact. The profile for NGC 2541 is fitted with a faint inner-truncated disk (the peak disk brightness is only about  $24 V - mag arcsec^{-2}$ ) and the hole radius is more than six disk scale lengths from the galaxy center. The southern half of the brightness profile contains a relatively bright spiral arm (about  $23 V - mag arcsec^{-2}$  at its brightest), and this asymmetry results in a bump in the averaged profile which has been fitted with the inner-truncation. NGC 5033 was fitted with a very faint ( $\mu_0 = 25.1 V - mag arcsec^{-2}$ ), very flat disk ( $r_0 = 732$  arcsec) which was never comparable in brightness to the bulge. As a result, the disk parameters for this galaxy are not well constrained by the data, and the estimated errors in the coefficients are correspondingly large. Finally, NGC 2997 has been fitted with a hole radius just smaller than the radius of the innermost data point, so the value of the hole radius is, again, not really constrained by the data.

Because of the presence of these extreme outliers, the median fractional errors are much more useful than the mean for examining the fitting errors of the sample as a whole. The summary in Table 4 shows that the median coefficient fractional errors range from a low of 1.6% for the disk scale length to more than 12% for the bulge effective intensity. From these data, it is clear that the bulge parameters are the least well determined quantities in the fits, while the disk parameters are generally well determined. This is not unexpected: since the bulge coefficients are usually dominated by a relatively small number of data points, the constraints on them are not very strong.

Finally, a few of the galaxies included in this study have been previously fitted by others with the same fitting functions, providing a completely independent check of the results of our fitting procedure. There are five galaxies in the current study which are also included in Boroson (1981), and 12 are in common with Kent (1985), making a total of 17 measurements available for use in this comparison. Prior to making any comparisons between the various works, the surface brightness parameters reported in Boroson (1981) and Kent (1985) have been "uncorrected" for the effects of inclination and galactic absorption as applied in each study, and the length parameters have been converted from kiloparsecs to arcseconds using the distances adopted by those authors. Furthermore, Boroson (1981) lists values for the disk  $B - V$  color, which have been used to convert his disk central surface brightnesses from the B bandpass to the V. Finally, there are two galaxies in common between Boroson (1981) and Kent (1985), and the same analysis has been applied to them. The percentage differences between the fitting parameters from these works and the present study have been computed and tabulated in Table 5. In this table, we list for each galaxy the percentage difference between the parameters in the referenced work and this

study, and also between the two reference works; the last column identifies the reference work. The differences were computed in the sense reference work minus this study, and Boroson minus Kent. These data are also presented in Figure 5, which shows the fitting parameters from Boroson (1981) and Kent (1985) plotted against the values obtained in the present study.

In general, the fits from the various studies do not agree very well, although the disk fits are typically more similar than the bulge fits. The mean of the absolute values of the percentage differences are 105% for  $I_e$ , 83% for  $r_e$ , 61% for  $I_0$ , and 26% for  $r_0$ , with 17 objects for all parameters. Our bulge fits agree somewhat better with those of Kent (1985), while our disk central surface brightnesses are closer to Boroson’s (1981) results – this reflects the conversion of Boroson’s surface brightnesses to the V-band. Interestingly, our values of  $r_0$  agree equally well, on average, with both reference works, leading us to believe that a 25% scatter in the disk scale length is to be expected under the circumstances of this comparison (differing bandpasses, .

The bulge fit differences are dominated by the effects of the profile acquisition procedures used in the different studies: this work used a wedge-shaped major axis cut, while Boroson (1981) and Kent (1985) used two variations on azimuthal averaging. In particular, it has been pointed out by Boroson (1981) that azimuthally averaged profiles will be systematically too bright in the bulge-dominated regions due to sampling the rounder bulge at a smaller galactocentric radius than the disk, at a given position in the image. Inspection of Table 5 reveals that every instance of a large departure in  $I_e$  shows a large departure in  $r_e$  of the *opposite* sign. That our bulge parameters agree better with Kent (1985) than with Boroson (1981) probably reflects the use of fixed ellipticities and position angles by Boroson, while Kent allowed those quantities to vary with radius. As a result, the mean surface brightness around ellipses in bulge-dominated regions are more representative of the major axis with Kent’s profile acquisition procedure than with Boroson’s, hence the slightly better agreement with our major axis cuts.

## 4. Fitting Characteristics

The basic result of the profile decomposition process is that 620 of the 659 profiles were successfully fitted with the chosen fitting functions. In this section, we will discuss some of the characteristics of the profile decomposition and the errors as they appear with this sample of galaxies. Our intent is to provide information regarding the characteristics of the fitting; we will present our analysis regarding the structure of disk galaxies elsewhere.

### 4.1. Fitting Parameters and Morphology

All galaxies included in this sample have lenticular or spiral RC3 Hubble types; however, 61 of the fits have been made with no disk component, indicating a lack of any appreciable exponential component to their brightness profiles. Visual inspection of these galaxies in the

PANBG shows many of them to have what appear to be disks even though the profile shows none (e.g., NGC 1784, NGC 1961, NGC 3370); others are possibly misclassified elliptical galaxies (e.g., NGC 2655, NGC 3998, NGC 5485). The galaxies with no disk component span a range in T-Type from -3 to 9 — the entire range of T-Type included in this sample. Early type galaxies are somewhat more likely to be fitted without a disk than are late types, but the trend is not very strong. There is no significant difference in the fit quality (as measured by the tabulated RMS deviation) between the galaxies without disk fits and the sample as a whole.

A total of 113 galaxies were fitted without a bulge component, and although these galaxies range in T-Type from -2 through 9, they are mostly late type galaxies. This, of course, is consistent with the basic behavior of the Hubble classification scheme where bulges are less prominent in later types. Again, the basic fitting quality is the same for galaxies without bulge fits as with the sample in general.

An investigation of the variation of the median fractional errors with T-Type is summarized in Table 6. This table gives for each range of T-Type the median fractional error of each fitting parameter, as well as the number of galaxies included in each median determination. The errors in  $I_e$ ,  $r_e$ , and  $I_0$  show some slight trends which are in the expected senses, but which are small enough to be of questionable significance. The two bulge parameters seem to have somewhat larger median errors for later types, as would be expected as the bulge contribution to the light distribution decreases. We should also note the work of Andredakis and Sanders (1994), who show that the inner regions of late-type spirals are perhaps better represented by an exponential light distribution than a deVaucouleurs’ law. Similarly, the disk central intensity error has larger values at earlier types, when the disk contribution is generally lower.

We also looked at the possibility of a fitting quality dependence on the presence or lack of a bar, and we have found nothing significant. The median RMS residual of the fits on non-barred galaxies (Hubble type in the RC3 contains an "A" explicitly) is about 0.14 magnitudes, for barred galaxies ("B") it is 0.15 magnitudes, for mixed types ("X") 0.16 magnitudes, and for objects with no bar classification given in the RC3 we find a value of 0.14 magnitudes. All of these values are sensibly the same as the median value of 0.15 magnitudes found for the full sample, and there is clearly no trend apparent. Table 7 lists the median fractional error of the individual fitting parameters for each bar class; there are no significant trends in these results. We conclude that bars have no discernable effect on the quality of the fits.

Objects which have been fitted with an inner truncation make up about 25% (156/620) of the sample. Remembering that inner truncations were included only if they improved the *weighted* RMS by at least 10%, this serves to justify our initial decision to use that function with this large data set. Some of these inner-truncations are probably caused by arms or rings at large galactocentric radii (e.g., NGC 2859, NGC 3368, and NGC 5701) – the arm/ring is bright relative to the local disk and thus mimics an inner-truncation. In these cases, the arm/ring is typically faint (peaks near  $24 V - mag \text{ arcsec}^{-2}$ ), and has a short disk scale length. These galaxies are also

generally classified as having an outer ring. These objects are identified in Table 1 with a "C" in the comment column. A more-detailed analysis of the presence of an inner-truncation is left for a later study.

#### 4.2. Fitting Parameters and Inclination

An analysis of the unweighted RMS residuals shows little or no trend in the mean value with inclination. We divided the sample into three inclination ranges based solely on the  $R_{25}$  value listed in the RC3, assuming that this isophote corresponds to a flat, circular disk:  $i \leq 30^\circ$  ( $R_{25} \leq 0.0625$ ),  $30^\circ < i \leq 60^\circ$  ( $0.0625 < R_{25} \leq 0.301$ ), and  $i > 60^\circ$  ( $R_{25} > 0.301$ ). Note that no T-Type dependence was included in this inclination estimate. The resulting mean RMS residuals for the low inclination, medium inclination, and high inclination samples are 0.16, 0.19, and 0.21 magnitudes, respectively. These three values are all much less than one standard deviation from each other, so the trend is statistically meaningless. The median RMS residuals for each inclination sample are 0.15 magnitudes, 0.14 magnitudes, and 0.17 magnitudes for the low, medium, and high inclinations, respectively. We conclude that the sample has no significant inclination dependence on the unweighted RMS residuals of the fits.

The quality of the individual fitting components is investigated by computing the median fractional errors within each inclination range; the mean fractional errors are not useful because of the outliers discussed previously. Table 8 provides the results of this investigation, which shows that there are no indications of any inclination dependencies. In Table 8, the first column lists the parameters, and the next three columns give the median relative errors in each inclination range.

Finally, we check if the rate of occurrence of the inner-truncation has any inclination dependence by computing the rate in each inclination range. The rates are  $28\% \pm 6.5\%$  for the low inclination group,  $28\% \pm 3.3\%$  for the medium inclinations, and  $19\% \pm 3.3\%$  for the high inclination sample. Thus, there is no trend significant at the  $2\sigma$  level.

### 5. Conclusions

We have presented one of the largest, if not the largest, collections of spiral and lenticular galaxy brightness profile bulge-disk decompositions yet completed. Of the 659 brightness profiles in our sample, 620 were fit with the deVaucouleurs law plus inner-truncated exponential disk function, while the remaining 39 profiles could not be so fit. The general quality of the fits is quite high, with about 50% of the fits having an unweighted RMS deviation from the data (including real structures) of less than 0.15 magnitudes and more than 90% have unweighted RMS residuals of less than 0.35 magnitudes. We find no systematic trends in the fitting quality with either galaxy morphology or inclination. Comparison of our fits with those of Boroson (1981) and Kent (1985) show discrepancies attributable to a number of observational and data reduction factors.

Probably the most interesting result from this process of fitting is simply that we achieved a "success" rate of 620/659 (94%) in our fits, compared to success rates of 75/94 (80%) for Kent (1985; spiral and S0 galaxies only) and 16/26 (62%) for Boroson (1981). While these success rates are statistically similar, we wonder if the small number statistics are the only differences. An analysis of the 19 non-fittable disk galaxy profiles from Kent (1985) shows that we found fits for all ten of those galaxies which were also in our sample. For these 10 objects, the mean inclination is  $41^\circ \pm 18^\circ$ , the median is  $42^\circ$ , and only one galaxy (NGC 5566) has an inclination greater than  $60^\circ$ . Thus, Kent's non-fittable galaxies do not tend to be high inclination objects. Furthermore, the RMS deviations of our fits for these same galaxies are generally small, with a median value of 0.15 magnitudes, the same as for our full sample. The principal difference seems to be that we included the inner-truncated disk (ITD) factor in our fits: seven of these 10 galaxies have ITD's in our fits, often with large  $r_h/r_0$  ratios. It is also possible that Kent's simultaneous fitting of the minor axis profiles made his results more sensitive to deviations from the standard fitting functions. A similar analysis of the 10 non-fittable profiles in Boroson's (1981) sample shows us having fits for the nine which are included in our sample. These nine galaxies are also of relatively low inclination (the largest is about  $58^\circ$ ), and have small RMS deviations in our fits (median value of 0.13 magnitudes). However, our fitted parameters show three objects with bulge only, three with a bulge plus exponential disk, and three with a bulge plus ITD; the case for the inclusion of the ITD is not as strong with this set of profiles. We conclude, however, that the inclusion of the ITD term in our fitting functions has allowed us to fit an additional 10% to 15% more galaxies than we would have fit without the inner-truncation term.

It is also interesting that about 25% of the profiles in our sample are fitted better by an inner-truncated disk function than with a plain exponential. Some of these fits are certainly due to the ITD being fitted to outer rings (as indicated by a "C" in the last column of Table 1), and others may be marginal improvements (remember the requirement for a 10% improvement of the *weighted* RMS to include the inner-truncation term), but clearly a significant fraction of the profiles support the physical reality of the inner-truncation in the light distribution. A quantification of the strength of the inner truncation and the search for the origin of this feature is the subject of a future paper.

Acknowledgements: One of the authors (WEB) has been supported by STScI under contract NAS5-26555 for this work. The authors would like to thank M. Hamabe for making the PANBG brightness profiles available to us for this project. We also wish to thank the anonymous referee for some useful suggestions. Part of the data analysis for this paper used STSDAS, which was developed by the Space Telescope Science Institute under U.S. Government contract NAS5-26555.

### A. Effects of Seeing on the Fitting Results

The fitting procedure described in section 3.1 makes no allowance for the effects of seeing other than to start the fitting at a radius larger than  $3''$  to avoid the most-affected portion of the brightness profile. We describe in this Appendix a set of experiments which were used to derive estimates of the correction factors for the fitted parameters to measure more accurately the true parameters of the bulge light distributions.

There are four factors in the profile acquisition process which can influence the fitting results, all of which occur at distinct stages of the process and which can be assumed to be separable. Seeing smears the galaxy light as it travels through the atmosphere, while Poisson noise occurs during the photographic exposure physics and chemistry. Pixellation broadens sharp features during the digitization of the plate, as well as adding some additional Poisson noise, and smearing by the aperture photometry happens as a result of the profile acquisition from the digitized data. Our experiments were designed to investigate only those processes which broaden sharp features of the galaxy light distribution: seeing, pixellation, and aperture photometry.

The PANBG provides seeing estimates for all plates in their Table 4.1; we assume that "seeing" in this case refers to the FWHM of stellar profiles. The tabulated seeing in the PANBG ranges from  $1''$  to  $7''$  and is included in our Table 1.

We attempted to replicate the profile definition process as accurately as possible utilizing computer-generated images. These images consist of a perfectly circular deVaucouleur's light distribution with input values of  $I_e = 1000$  in arbitrary intensity units and  $r_e = 0.5, 1, 2, 4, 8, 16,$  and  $32''$ . Poisson noise was included in the images. No disk component was included in these images because the most pronounced effects of seeing will be on the bulge component due to its very steep slope at small radii. We generated  $512 \times 512$  pixel images with these characteristics, assuming a pixel scale of 3 pixels/ $''$  (to simulate the photographic resolution), then smeared them with Gaussians of FWHM=1, 2, 3, 4, 5, 6, and  $7''$  to simulate the effect of the atmosphere during a long exposure. The resulting images were then block averaged with a  $3 \times 3$  pixel ( $1''$  square) block to replicate the plate scanning utilized for most of the galaxies in the PANBG. Finally, the brightness profiles from the simulated images were extracted using a set of variable diameter circular apertures along a single radius of the "galaxies." These profiles were then fitted in the same fashion as the real profiles in order to estimate the functional parameters, using a fixed fitting range of  $3''$  to  $48''$ . A second set of images was generated using the same input parameters, but which were not smeared by the Gaussians; these images were used to determine the correction factors due to the pixellation and profile acquisition aperture photometry prior to estimating the effects of smearing with a Gaussian.

The results of this procedure are presented in Table 9, which includes for each simulation the seeing size in arcseconds, the input  $I_e$  and  $r_e$ , the fitted  $I_e$  and  $r_e$ , and the ratio of each fitted parameter to its input value, all based on the fully-degraded brightness profiles. The  $I_e$  are all in arbitrary intensity units, and the  $r_e$  are all in simulated arcseconds. Figure A1 shows

the relationship between the fitted:input  $I_e$  as a function of the fitted:input  $r_e$ ; the two quantities are highly anti-correlated, suggesting that the fitted parameters are not truly independent of one another.

As can be seen from the table, there are some cases where the fitted parameters are very different from the input values: the worst cases, as would be expected, are where the seeing disk is large compared to the input  $r_e$ . For  $r_e$ , the percent errors range from less than 1% to almost 40% (seeing=7",  $r_e = 1''$ ), while for  $I_e$  the range is from almost 0% (seeing=4",  $r_e = 32''$ ) to more than 1000% (seeing=7",  $r_e = 1''$ ). We have every reason to suspect that similar fitting errors exist in the PANBG fits, and a means of correcting these errors is highly desirable.

The correction procedure has been separated into two stages: first correct the fitted parameters for the combined effects of pixellation and aperture photometry, then correct these modified parameters for the effects of the Gaussian smearing. The pixellation/aperture photometry correction for the effective radius, based on the simulations without Gaussian smearing, has been found to be well-represented by a power law of the form

$$\log(r'_e/r_e) = 0.005\log(b/r_e) - 0.018 \quad (\text{A1})$$

or

$$r'_e = 0.959r_e(b/r_e)^{0.005} \quad (\text{A2})$$

where  $r_e$  is the fitted effective radius,  $b$  is the digitization aperture size (1"), and  $r'_e$  is the effective radius corrected for the effects of pixellation and aperture photometry; the units of all quantities are in arcsec. This function has a correlation coefficient of 0.989, and a maximum percentage error of 0.2% within the parameter space studied.

The pixellation/aperture correction function for the effective intensity is similarly found to be

$$I'_e = [0.068\log(b/r_e) + 1.246]I_e \quad (\text{A3})$$

where  $I_e$  is the fitted effective intensity,  $r_e$  is the fitted effective radius,  $b$  is the digitization aperture size, and  $I'_e$  is the effective intensity corrected for pixellation and aperture photometry. This function has a correlation coefficient of 0.995 and a maximum percentage error of 0.6% within the parameter space studied. Figure A2 shows the fits of the pixellation/aperture photometry correction functions for both  $r_e$  and  $I_e$ .

The seeing correction is applied by the linear interpolation of the galaxy parameters on the model parameters for the same value of seeing. In Table 10 we list the model data used in the interpolation; column 1 lists the seeing in arcsec ( $S$ ), column 2 the ratio of the seeing to the pixellation-corrected effective radius ( $S/r'_e$ ), column 3 the ratio of the input effective intensity

to the pixellation-corrected effective intensity ( $I_e^0/I_e'$ ), and column 4 the ratio of the input effective radius to the pixellation-corrected effective radius ( $r_e^0/r_e'$ ). The interpolation procedure is performed by computing the  $S/r_e'$  ratio for a fit, and interpolating the  $I_e^0/I_e'$  and  $r_e^0/r_e'$  ratios for the tabulated seeing disk size to derive the fully-corrected  $I_e^0$  and  $r_e^0$  from the previously-computed values of  $I_e'$  and  $r_e'$  (eqs. A2 and A3).

We include in Table 1 the corrected bulge parameters resulting from the described correction procedure. Corrections for objects whose fitted parameters lie outside of the interpolation parameter space are not provided in Table 1.

## REFERENCES

- Andredakis, Y.C., Peletier, R.F., and Balcells, M. 1995, MNRAS, 275, 874
- Andreyakis, Y.C. and Sanders, R.H. 1994, MNRAS, 267, 283
- Baggett, W.E., Baggett, S.M., and Anderson, K.S.J. 1993, BAAS, 24, 1223
- Bevington, P.R. 1969, *Data Reduction and Error Analysis for the Physical Sciences*, (McGraw-Hill Book Company, New York), p 184
- Boroson, T. 1981, ApJS, 46, 177
- Burstein, D. 1979, ApJ, 234, 435
- Byun, Y.I., and Freeman, K.C. 1995, ApJ, 448, 563
- deJong, R. 1996, A&A, 313, 45
- Freeman, K.C. 1970, ApJ, 160, 811
- Holmberg, E. 1947, Medd. Lund. Astr. Obs., Ser. 2, No. 120
- Hubble, E. 1930, ApJ, 71, 231
- Kent, S. 1985, ApJS, 59, 115
- King, I.R. 1966, AJ, 71, 64
- Kodaira, K., Okamura, S., and Ichikawa, S. (eds.) 1990, *Photometric Atlas of Northern Bright Galaxies*, (University of Tokyo Press, Tokyo) (PANBG)
- Kormendy, J. 1977, ApJ, 217 406
- Longo, G. and deVaucouleurs, A. 1983, *The University of Texas Monograph in Astronomy*, No. 3, (University of Texas, Austin)
- Sandage, A. 1961, *The Hubble Atlas of Galaxies*, (Carnegie Institution of Washington, Washington)
- Sandage, A. and Tammann, A. 1981, *A Revised Shapley-Ames Catalog of Bright Galaxies*, (Carnegie Institution of Washington, Washington) (RSA)
- deVaucouleurs, G. 1953, MNRAS, 113, 134



deVaucouleurs, G., deVaucouleurs, A., Corwin, H.G., Buta, R.J., Paturel, G., and Fouque, P.  
1991, *Third Reference Catalogue of Bright Galaxies*, (Springer-Verlag, New York)

Fig. 1.— Brightness profile fits to the NGC 3145 data. Both plots show the bulge component, the disk component, and the sum of the two. The horizontal line at  $25.3 V - mag arcsec^{-2}$  indicates the range of radius included in the fit. *Left:* Fit without a truncation term in the disk component; the RMS deviation of this fit is 0.28 mag. *Right:* Fit including the truncation term in the disk component; the RMS deviation of this fit is 0.12 mag.

Fig. 2.— Brightness profile fits to the galaxies presented in Table 1. Each plot shows the observed profile (crosses), the bulge and disk components and their sum (solid lines), and the range of radius included in the fit (horizontal line(s) at bottom). Also shown are the fitted parameters, where the surface brightness parameters are in units of  $V - mag arcsec^{-2}$  and the size parameters are in arcseconds.

Fig. 3.— Distribution of RMS deviations of the fits from the data. The RMS deviations were computed for all data points in each profile between 3 arcsec and the first point at which the surface brightness drops below  $25 V - mag arcsec^{-2}$ . The median value of the distribution is at 0.15 mag. There are six objects which have RMS deviations greater than 1.0 mag which are not included in the figure.

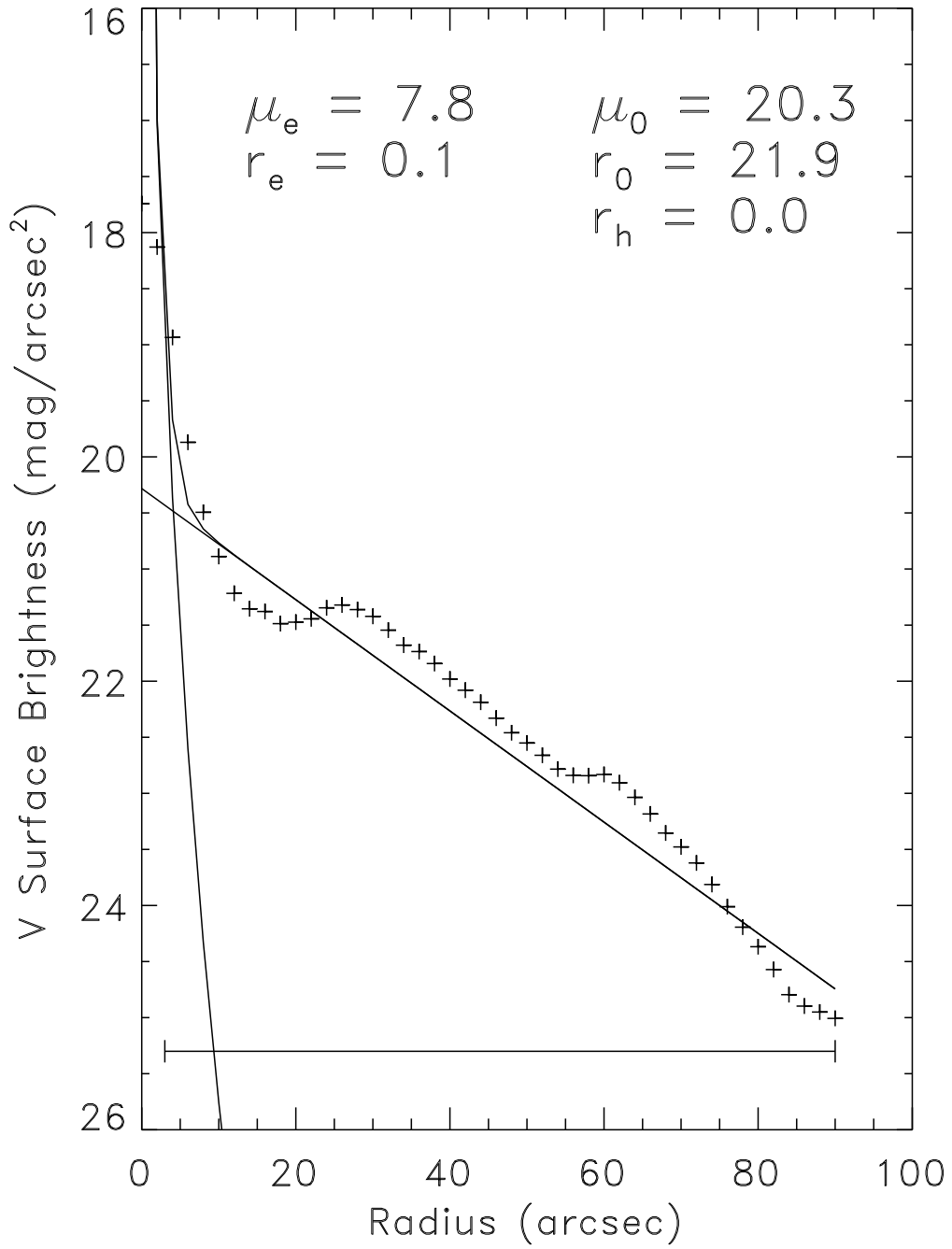
Fig. 4.— Histograms of the fractional errors. The distributions of the estimated fractional errors of each fitted parameter are shown to illustrate the problem with outliers: a)  $I_e$ , b)  $r_e$ , c)  $I_0$ , d)  $r_0$ , and e)  $r_h$ . Note the smaller bin size for  $r_0$  and  $r_h$ .

Fig. 5.— Comparison of fitted parameters. The fit parameters for the galaxies in common with Boroson (1981) (plus signs) and Kent (1985) (asterisks) are shown along with the 45-degree line. The surface brightness parameters are expressed in units of  $mag arcsec^{-2}$  and the length parameters are given in  $arcsec$ . There is a reasonable correlation for all of the parameters, although the disk parameters have tighter correlations than those for the bulge.

Fig. 6.— Relationship between  $I_e$  fitting accuracy and  $r_e$  fitting accuracy. The apparent anticorrelation suggests some dependence of the fitting parameters on each other.

Fig. 7.— Pixellation/aperture photometry correction functions. a) The data and fit for the correction function for  $r_e$  is shown in a log-log plot. There is clearly a systematic residual function, but it is of insignificant amplitude. b) The data and fit for the  $I_e$  correction function is shown; again there is an insignificant systematic residual, particularly at large values of  $b/r_e$ .

# N3145



# N3145

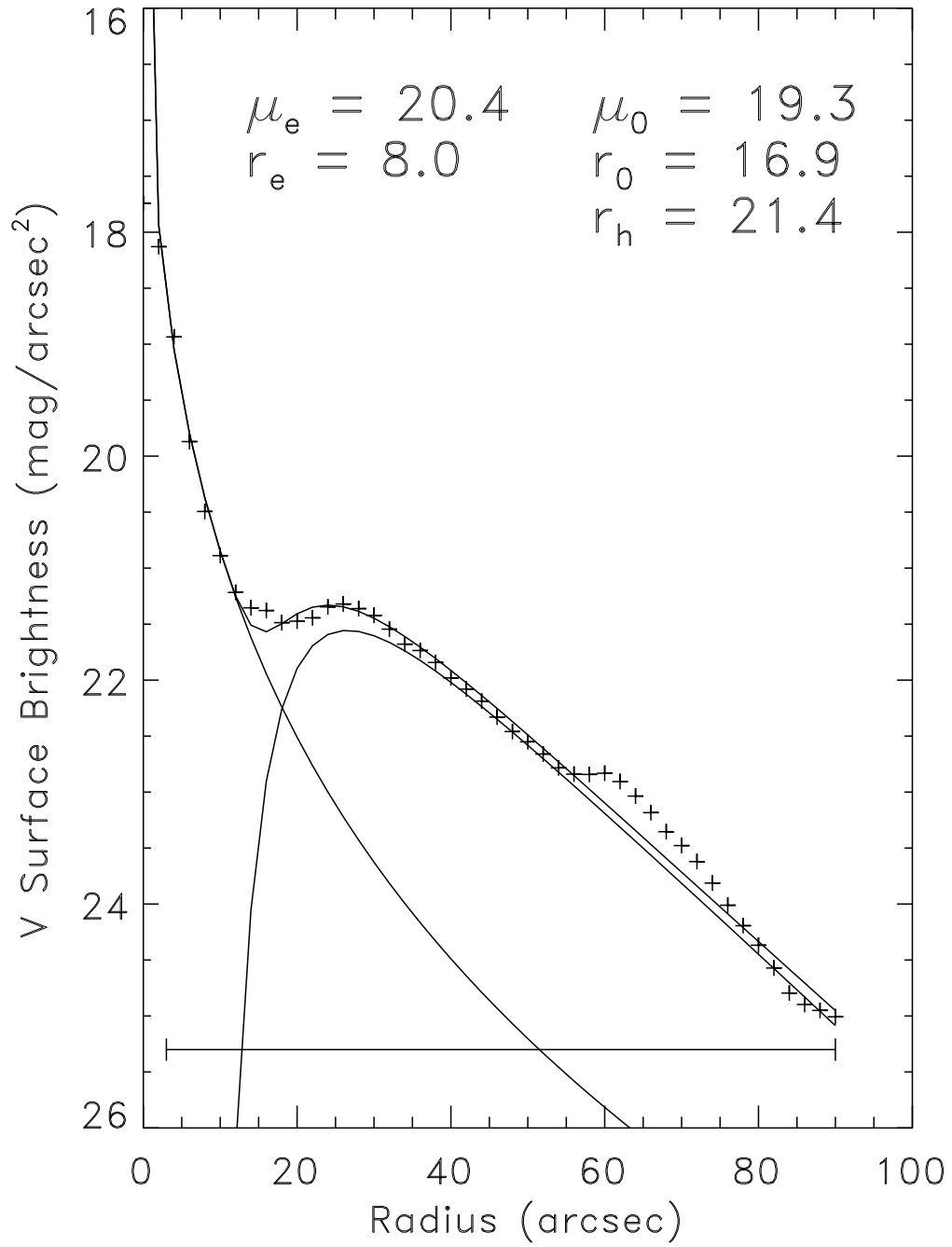


TABLE 1. Sample Galaxy Fit Parameters

Galaxy <sup>a</sup>	Type <sup>b</sup>	T <sup>c</sup>	$R_{25}$ <sup>d</sup>	Range <sup>e</sup>	$\mu_e$ <sup>f</sup>	$r_e$ <sup>g</sup>	$\mu_0$ <sup>h</sup>	$r_0$ <sup>i</sup>	$r_h$ <sup>j</sup>	RMS <sup>k</sup>	Seeing <sup>l</sup>	$\mu_e^{0m}$	$r_e^{0n}$	Notes <sup>o</sup>
N0016	.LX.-./	-3	0.27	3.:70.	20.83	13	22.41	18.8	...	0.07	1	20.67	12.37	
N0023	.SBS1..	1	0.19	3.:58.	7.18	0.1	19.83	11.5	...	0.21	1	...	...	D
N0148	.L..0*/	-2	0.4	3.:68.	12.3	0.4	19.24	12.5	...	0.11	5	13.64	0.5	
N0151	.SBR4..	4	0.34	3.:65.	17.95	2.4	20.93	34.4	...	0.54	2	17.88	2.37	A,E
N0157	.SXT4..	4	0.19	3.:11.,92.:148.	20.85	7.2	20.56	35.8	...	0.51	2	20.74	7.01	A
N0224	.SAS3..	3	0.49	100.:5600.	19.89	282.2	20.58	1781.2	...	0.13	4	...	...	
N0237	.SXT6..	6	0.24	3.:8.,27.:50.	...	...	19.99	10.4	...	0.17	2	...	...	A
N0245	.SAT3P\$	3	0.06	3.:46.	20.11	3.9	19.24	8.8	10.1	0.12	2	20.02	3.82	
N0253	.SXS5..	5	0.61	3.:276.,725.:936.	21.19	18.7	19.51	192.3	...	0.4	5	21.3	19.73	A
N0254	RLXR+*	-1	0.21	3.:82.	15.94	1.4	20.09	18.5	...	0.12	5	16.93	1.75	
N0255	.SXT4..	4	0.08	3.:70.	21.98	12	19.97	14.7	12.5	0.12	2	21.87	11.61	
N0268	.SBS4*.	4	0.14	3.:52.	...	...	19.86	11.2	...	0.25	3	...	...	D
N0274	.LXR-P.	-3	0.01	4.:40.	16.67	2	16.79	5	17.5	0.22	3	16.87	2.11	I
N0278	.SXT3..	3	0.02	3.:102.	20.36	17.1	...	...	...	0.19	3	20.32	16.95	
N0289	.SBT4..	4	0.15	3.:60.	...	...	18.81	14	...	1.12	5	...	...	A,D
N0309	.SXR5..	5	0.08	3.:74.	11.88	0.2	20.9	21.4	...	0.25	3	...	...	
N0357	.SBR0*.	0	0.14	3.:19.,57.:80.	18.5	3.5	22.35	31.5	...	0.38	3	18.6	3.62	A,E
N0404	.LAS-*.	-3	0	3.:288.	22.15	63.8	23.02	129.5	...	0.09	2	22.05	60.86	
N0428	.SXS9..	9	0.12	4.:92.	...	...	20.19	20.7	...	0.12	5	...	...	
N0473	.SXR0*.	0	0.2	3.:58.	19.22	4.2	20.44	13.8	...	0.1	5	19.69	4.85	

TABLE 1. (continued)

Galaxy <sup>a</sup>	Type <sup>b</sup>	T <sup>c</sup>	$R_{25}$ <sup>d</sup>	Range <sup>e</sup>	$\mu_e$ <sup>f</sup>	$r_e$ <sup>g</sup>	$\mu_0$ <sup>h</sup>	$r_0$ <sup>i</sup>	$r_h$ <sup>j</sup>	RMS <sup>k</sup>	Seeing <sup>l</sup>	$\mu_e^{0m}$	$r_e^{0n}$	Notes <sup>o</sup>
N0514	.SXT5..	5	0.1	3.:94.	24.17	38.5	20.97	24.4	13.2	0.12	5	24.21	39.51	
N0521	.SBR4..	4	0.04	3.:94.	21.26	10.9	20.9	26.6	20.8	0.1	5	21.46	11.82	F
N0524	.LAT+..	-1	0	4:136.	21.47	33.6	...	...	...	0.11	3	21.41	32.92	
N0598	.SAS6..	6	0.23	3.:2256.	22.71	109.6	20.3	533.3	...	0.12	2	...	...	

<sup>a</sup>Galaxy ID – N=NGC, I=IC

<sup>b</sup>Revised Hubble type from RC3

<sup>c</sup>T-type from RC3

<sup>d</sup> $R_{25}[= \log(a/b)]$  from RC3

<sup>e</sup>Fitting range(s), in units of arcseconds

<sup>f</sup>Bulge effective surface brightness in  $V - mag \text{ arcsec}^{-2}$

<sup>g</sup>Bulge effective radius in units of arcseconds

<sup>h</sup>Disk central surface brightness in  $V - mag \text{ arcsec}^{-2}$

<sup>i</sup>Disk scale length in units of arcseconds

<sup>j</sup>Disk truncation radius in units of arcseconds

<sup>k</sup>RMS deviation of the fit in  $V - mag \text{ arcsec}^{-2}$

<sup>l</sup>Seeing in arcseconds from PANBG

<sup>m</sup>Fully-corrected bulge effective surface brightness in  $V - mag \text{ arcsec}^{-2}$

<sup>n</sup>Fully corrected bulge effective radius in units of arcseconds

<sup>o</sup>Notes about individual galaxies

Notes to Table 1.

A – Prominent arm/bar/ring/dust lane removed from fit.

B – Much structure in profile.

C – Truncated disk fit to a bright arm or lens.

D – Bar near major axis.

E – Bar near minor axis.

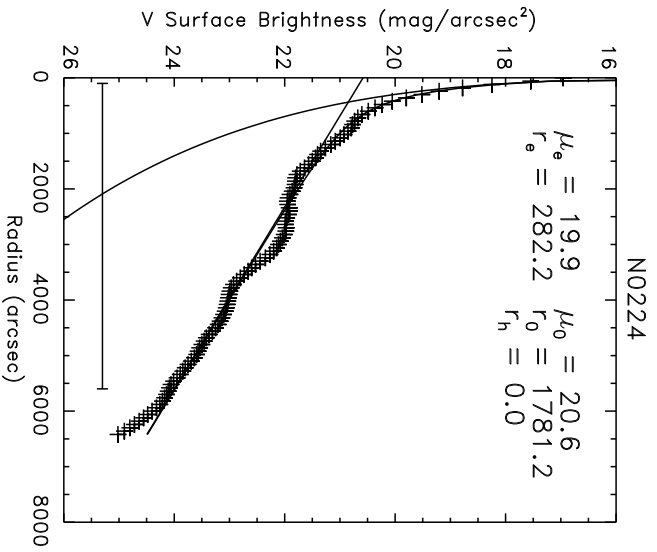
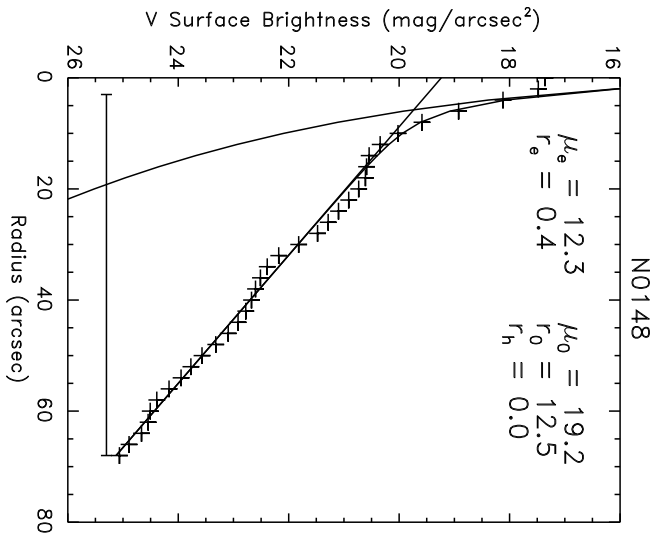
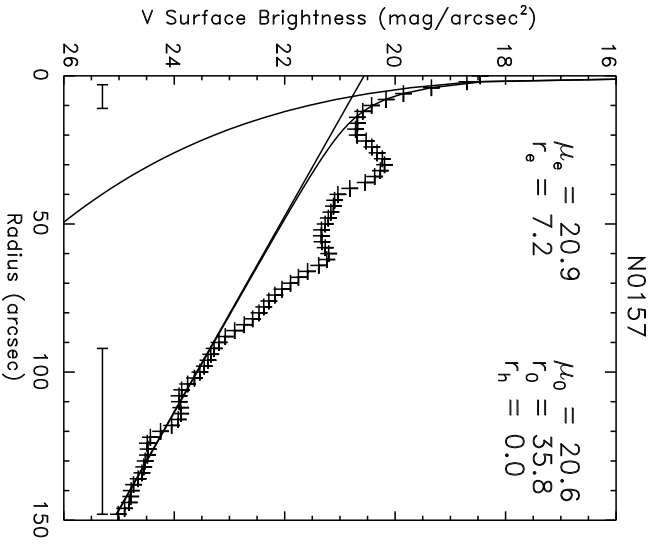
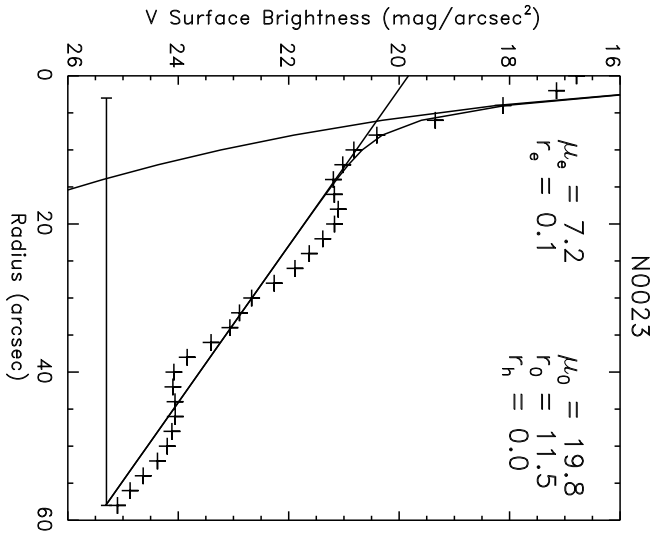
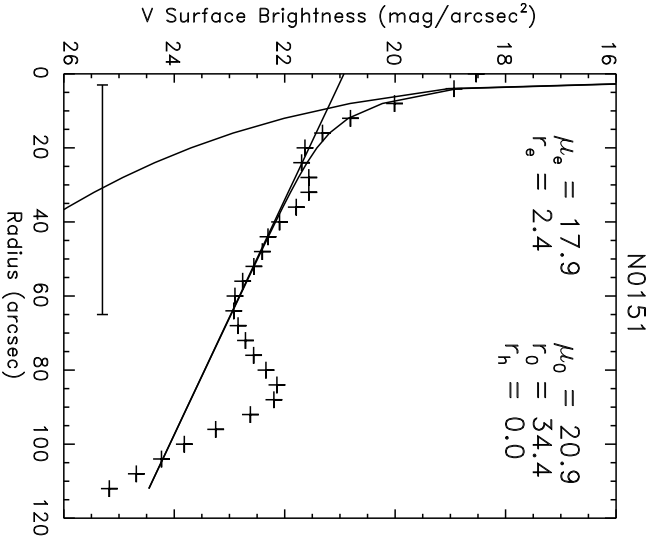
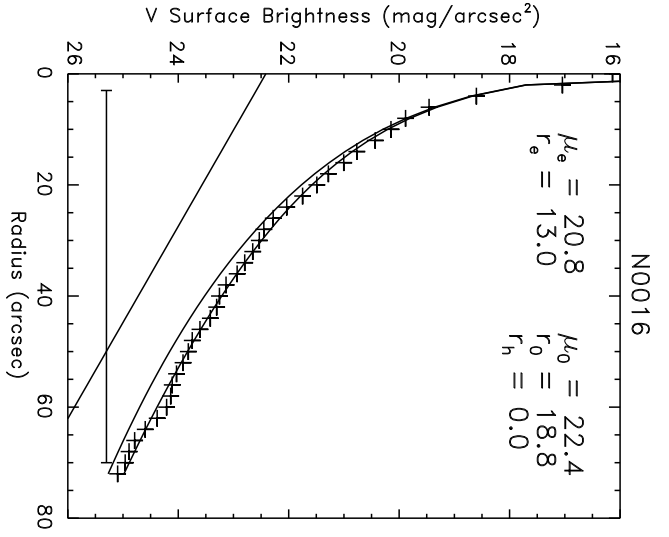
F – Bar between axes.

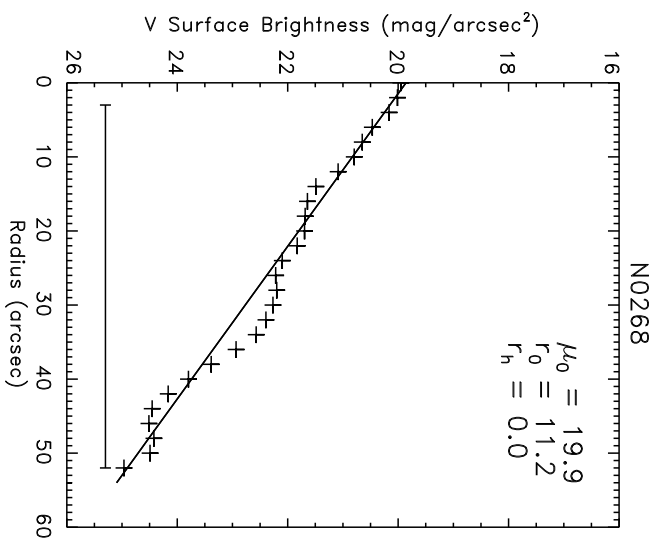
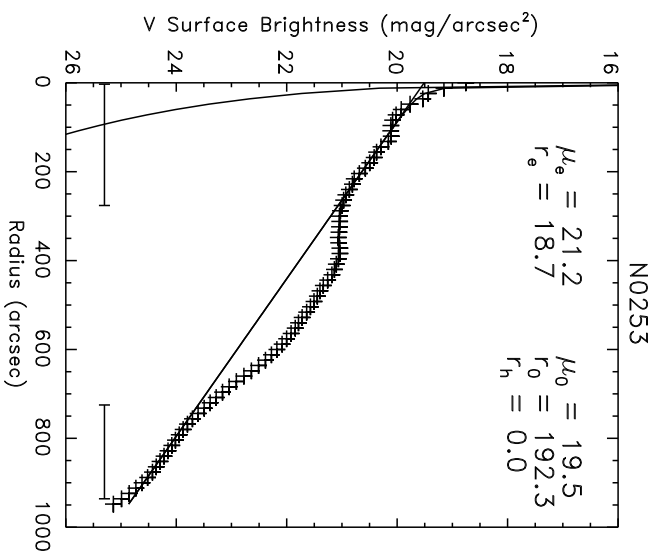
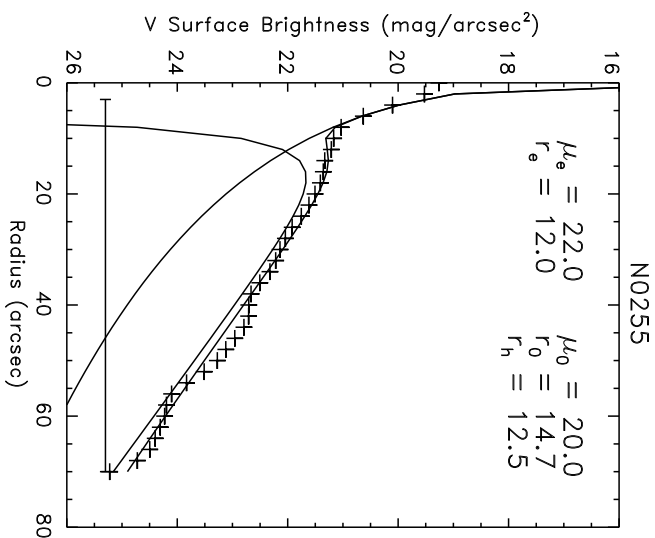
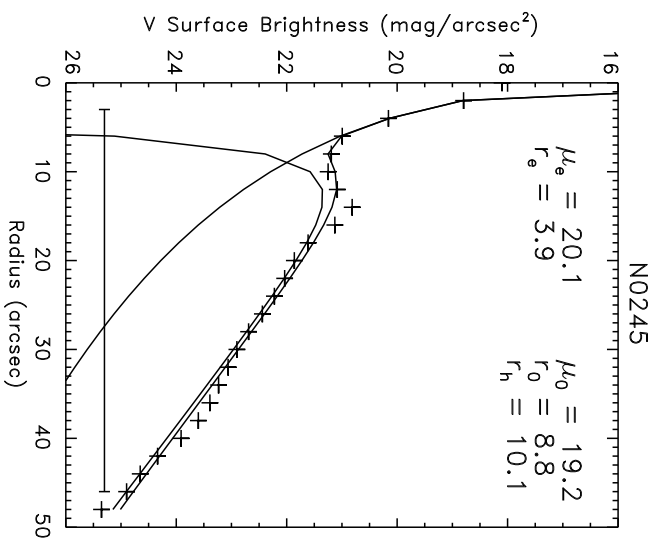
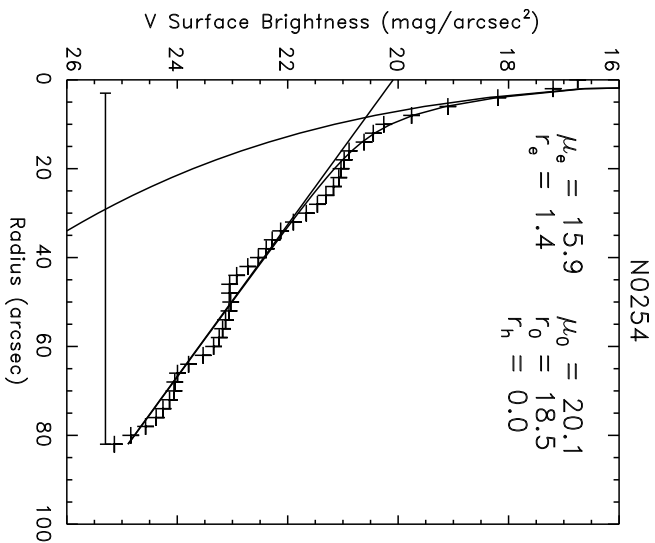
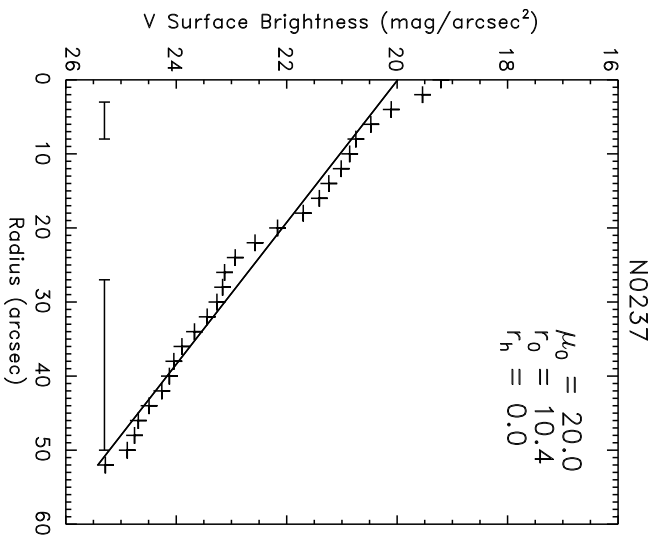
G – Edge-on.

H – Box/peanut bulge evident in published image.

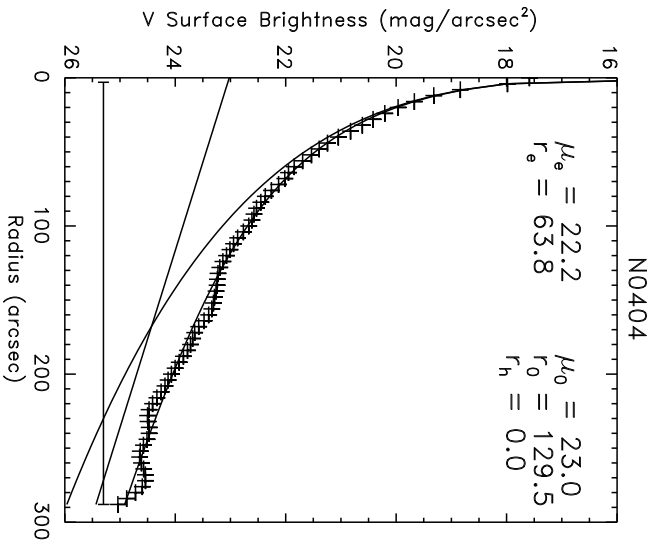
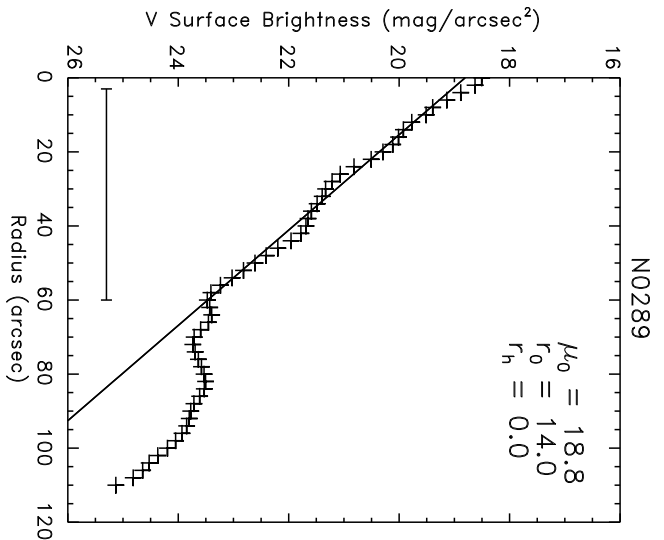
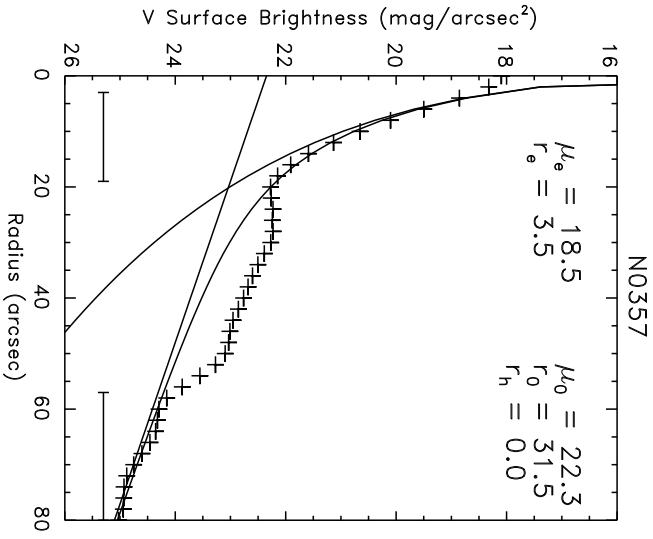
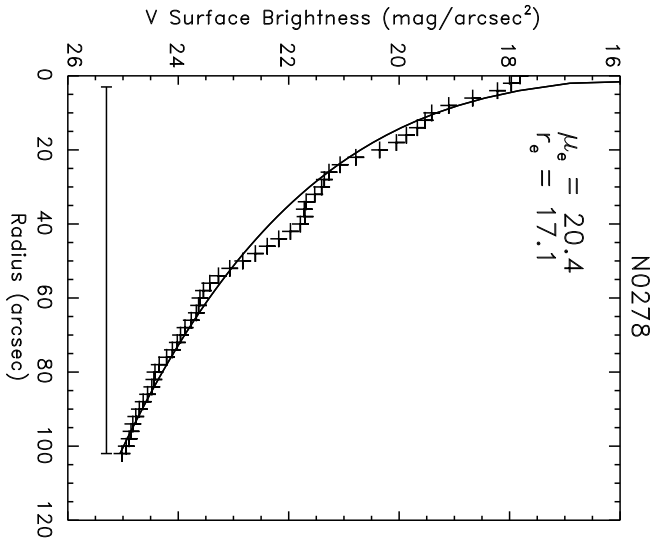
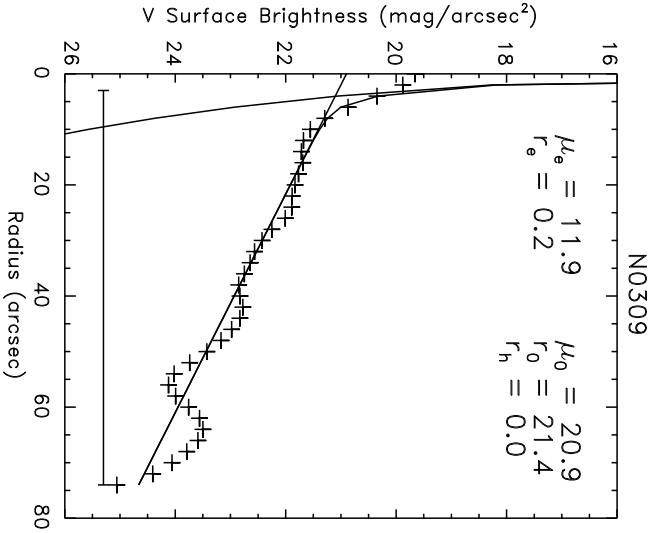
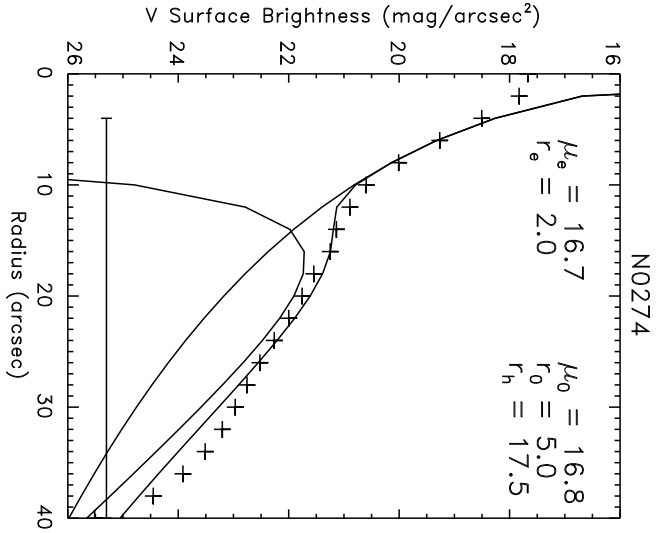
I – Interacting.

J – NGC 4891 is not included in the RC3, but it appears to be listed as NGC 4897. The RC3 data listed is that for NGC 4897.









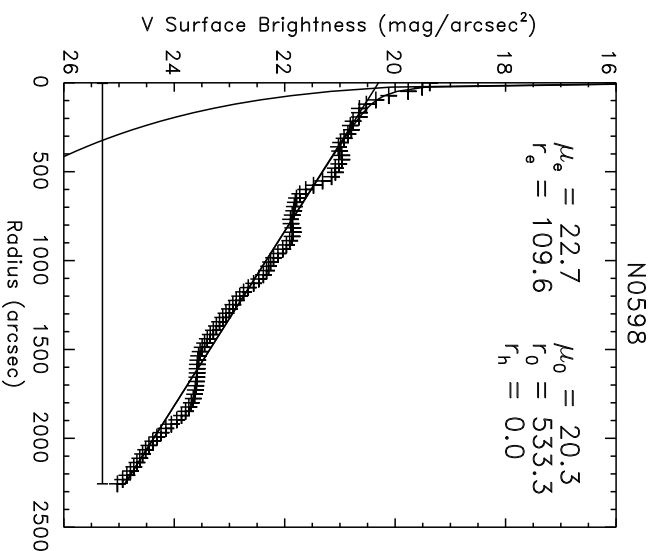
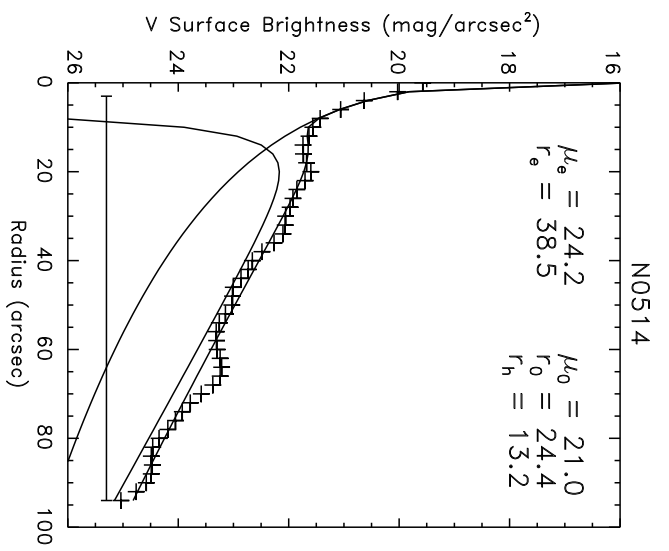
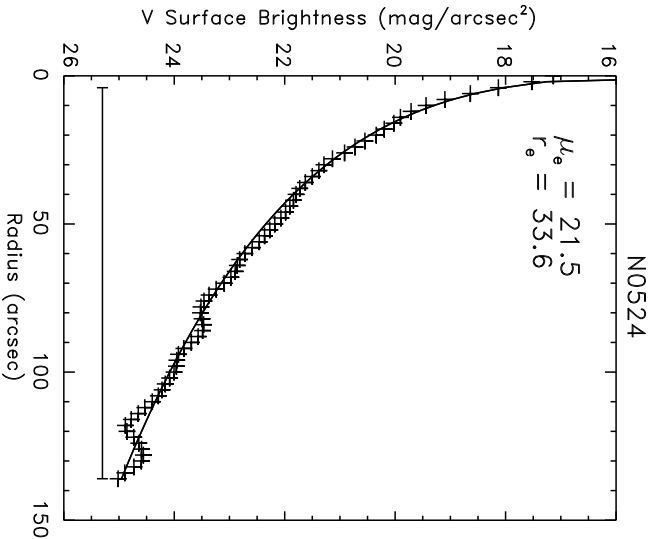
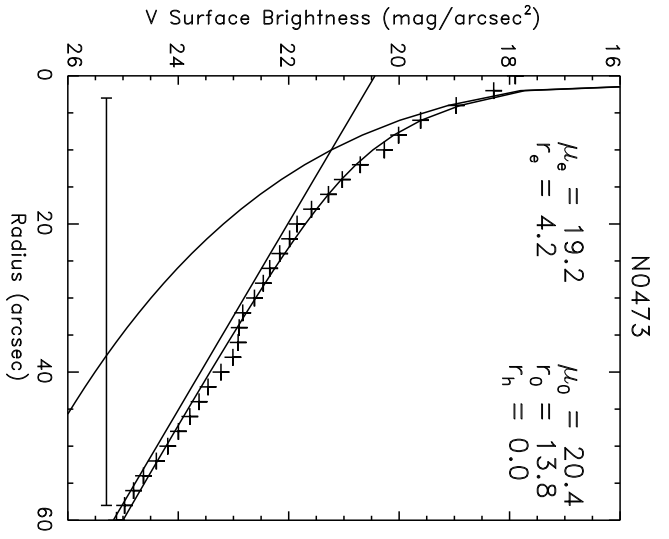
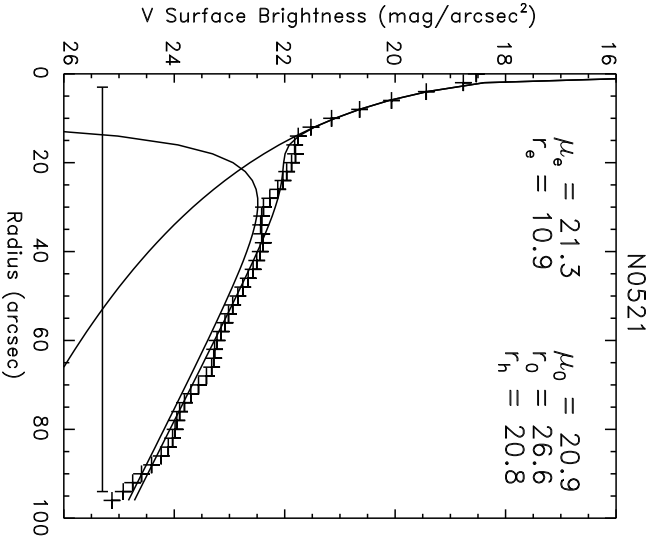
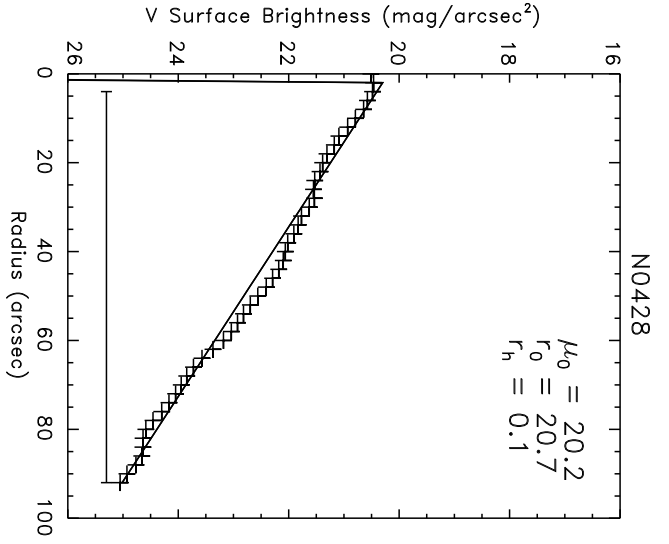


TABLE 2. Non-Fitted Galaxies

Galaxy	Type	$R_{25}$	Comments
N0150	.SBT3*	0.32	Very bright arms at $r \sim 50''$
N0275	.SBT6P.	0.14	Concave to low $\mu$ (ITD with no bulge?)
N0337	.SBS7..	0.20	Concave to low $\mu$
N0908	.SAS5..	0.36	Exp. disk truncated at $\sim 150''$
N0941	.SXT5..	0.13	Strong structure in outer profile
N1035	.SAS5\$.	0.48	Concave to low $\mu$
N1358	.SXR0..	0.10	Large, bright plateau with sharp outer cutoff
N1667	.SXR5..	0.11	Three exponentials?
N2146	.SBS2P.	0.25	Very disturbed galaxy
N2633	.SBS3..	0.20	Strong structure throughout profile
N2793	.SBS9P.	0.07	Very asymmetric profile
N2976	.SA.5P.	0.34	Concave to low $\mu$
N2990	.S..5*.	0.27	Concave to low $\mu$
N3003	.S..4\$.	0.63	Strong structure throughout profile
N3021	.SAT4*.	0.25	Concave to low $\mu$
N3043	.S..3*/	0.48	Concave to low $\mu$
N3067	.SXS2\$.	0.42	Concave to low $\mu$
N3312	.SAS3P\$	0.42	Large, bright plateau with sharp outer cutoff
N3432	.SBS9./	0.66	Strong structure throughout profile
N3455	PSXT3..	0.21	Concave to low $\mu$ , faint outer extension
N3556	.SBS6./	0.59	Strong structure throughout profile
N3628	.S..3P/	0.70	Disturbed edge-on system
N3664	.SBS9P.	0.03	Strong structure throughout profile
N3717	.SA.3*/	0.73	Double exponential, edge-on
N3810	.SAT5..	0.15	Strong structure in outer profile
N4013	.S..3./	0.71	Concave to low $\mu$ , edge-on
N4085	.SXS5*\$	0.55	Concave to low $\mu$
N4302	.S..5*/	0.74	Extremely edge-on
N4487	.SXT6..	0.17	Double exponential
N4517	.SAS6*/	0.83	Extremely edge-on
N4618	.SBT9..	0.09	Strong structure in outer profile
N5112	.SBT6..	0.15	Strong structure in outer profile
N5170	.SAS5*/	0.91	Concave to low $\mu$ , edge-on
N5301	.SAS4*/	0.69	Strong structure in outer profile
N5474	.SAS6P.	0.05	Very asymmetric profile
N5746	.SXT3\$/\$	0.75	Concave to low $\mu$ , edge-on
N5775	.SB.5\$/\$	0.62	Concave to low $\mu$ , edge-on
N5949	.SAR4\$.	0.33	Concave to low $\mu$
I0764	.SAS5\$.	0.47	Strong structure throughout profile

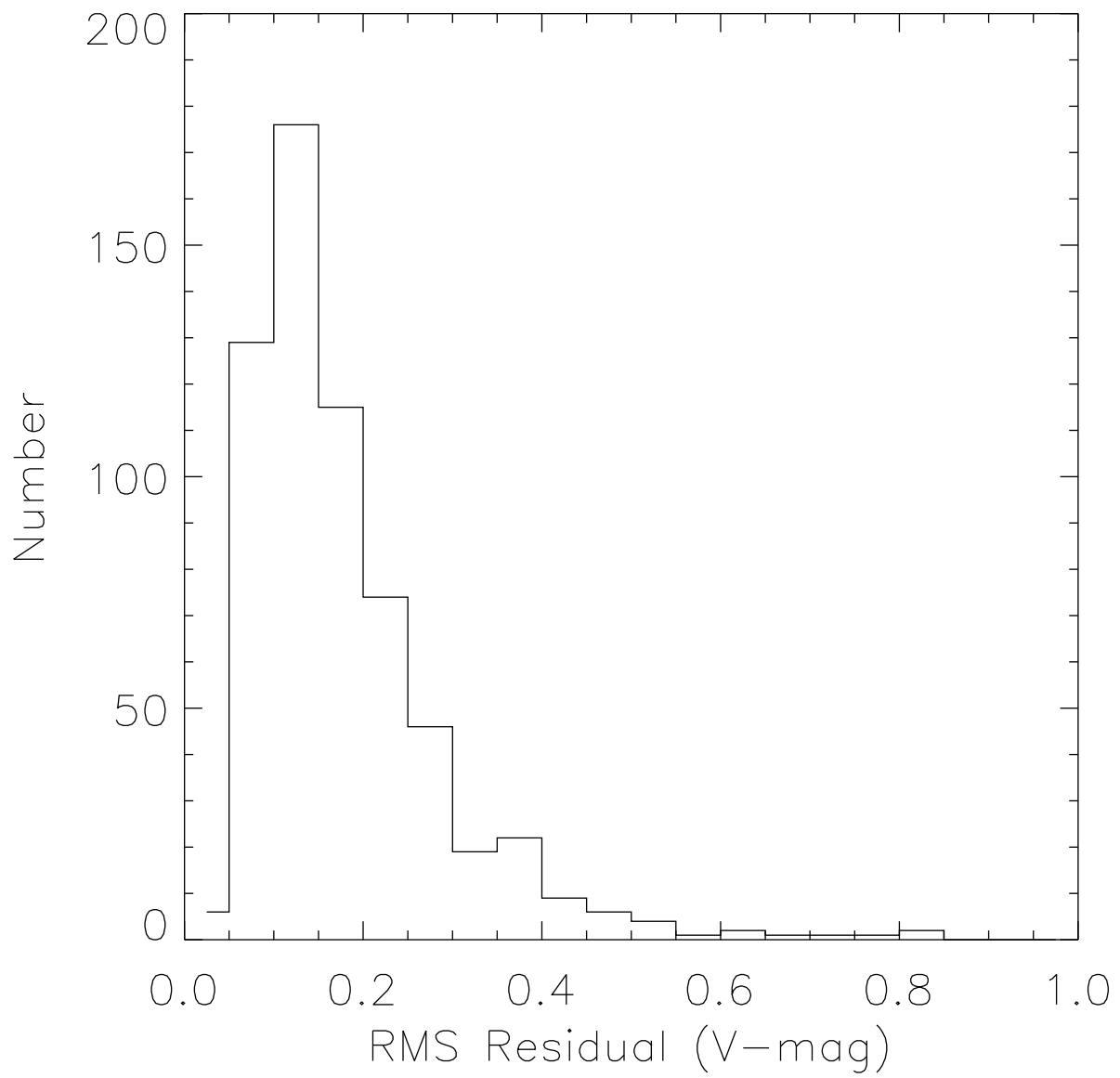


TABLE 3. Parameter Fractional Errors

Galaxy	$\Delta(I_e)$	$\Delta(r_e)$	$\Delta(I_0)$	$\Delta(r_0)$	$\Delta(r_h)$
N0016	0.212	0.125	0.447	0.087	...
N0023	0.365	0.094	0.023	0.008	...
N0148	0.520	0.157	0.031	0.012	...
N0151	0.255	0.099	0.044	0.035	...
N0157	0.601	0.380	0.117	0.035	...
N0224	0.078	0.047	0.018	0.010	...
N0237	...	...	0.023	0.010	...
N0245	0.337	0.165	0.053	0.018	0.019
N0253	0.671	0.350	0.010	0.007	...
N0254	0.258	0.110	0.038	0.014	...
N0255	0.250	0.174	0.035	0.018	0.021
N0268	...	...	0.012	0.008	...
N0274	0.117	0.053	0.154	0.028	0.015
N0278	0.026	0.014	...	...	...
N0289	...	...	0.007	0.004	...
N0309	4.950	0.620	0.021	0.014	...
N0357	0.257	0.121	0.230	0.115	...
N0404	0.057	0.052	0.158	0.080	...
N0428	...	...	0.010	0.007	...
N0473	0.365	0.307	0.114	0.014	...
N0514	0.227	0.248	0.032	0.028	0.036
N0521	0.070	0.042	0.038	0.017	0.021
N0524	0.024	0.014	...	...	...

Notes to Table 3.

Column headings:

Col. 1 – Galaxy ID (N=NGC, I=IC)

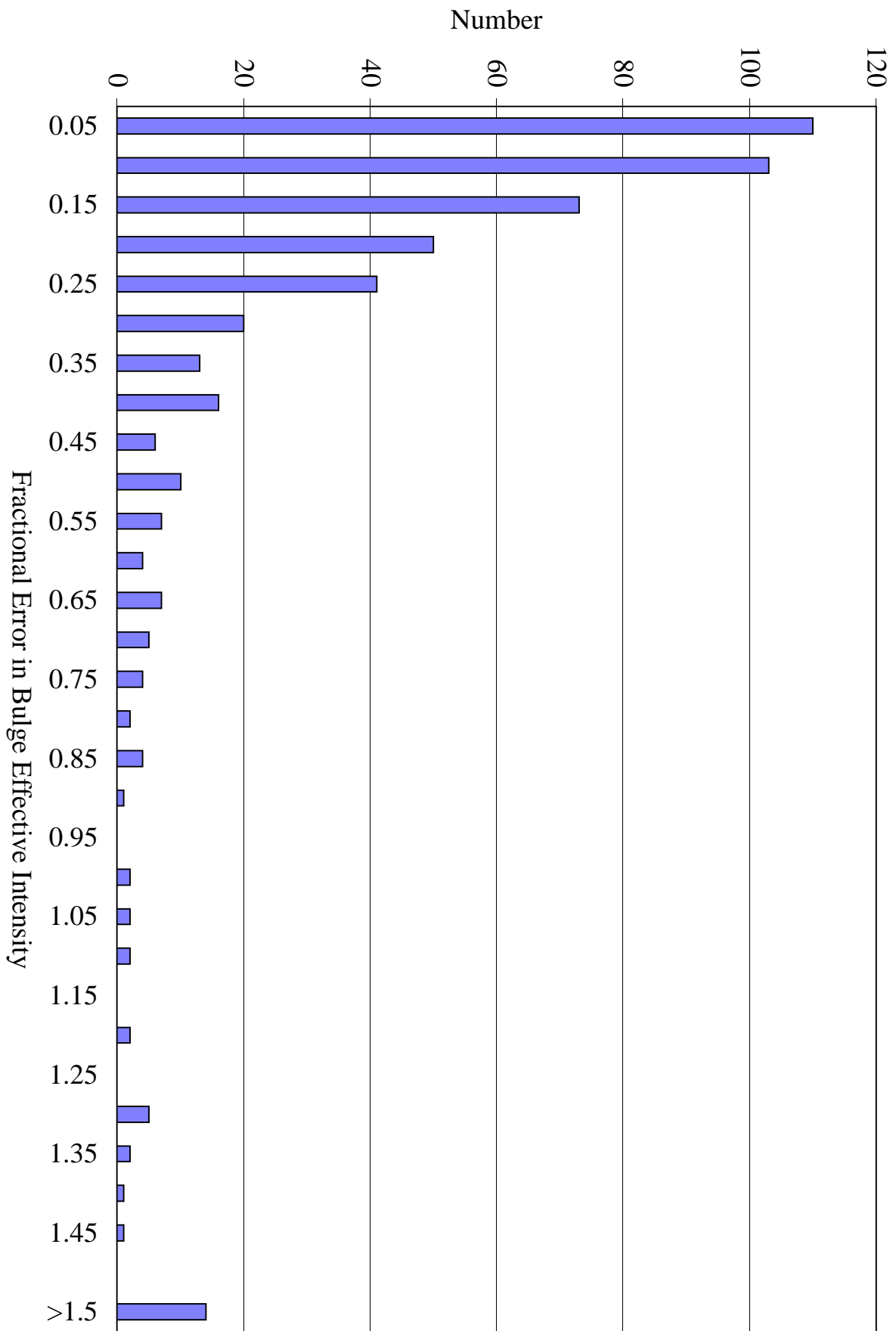
Col. 2 – Fractional error in  $I_e$

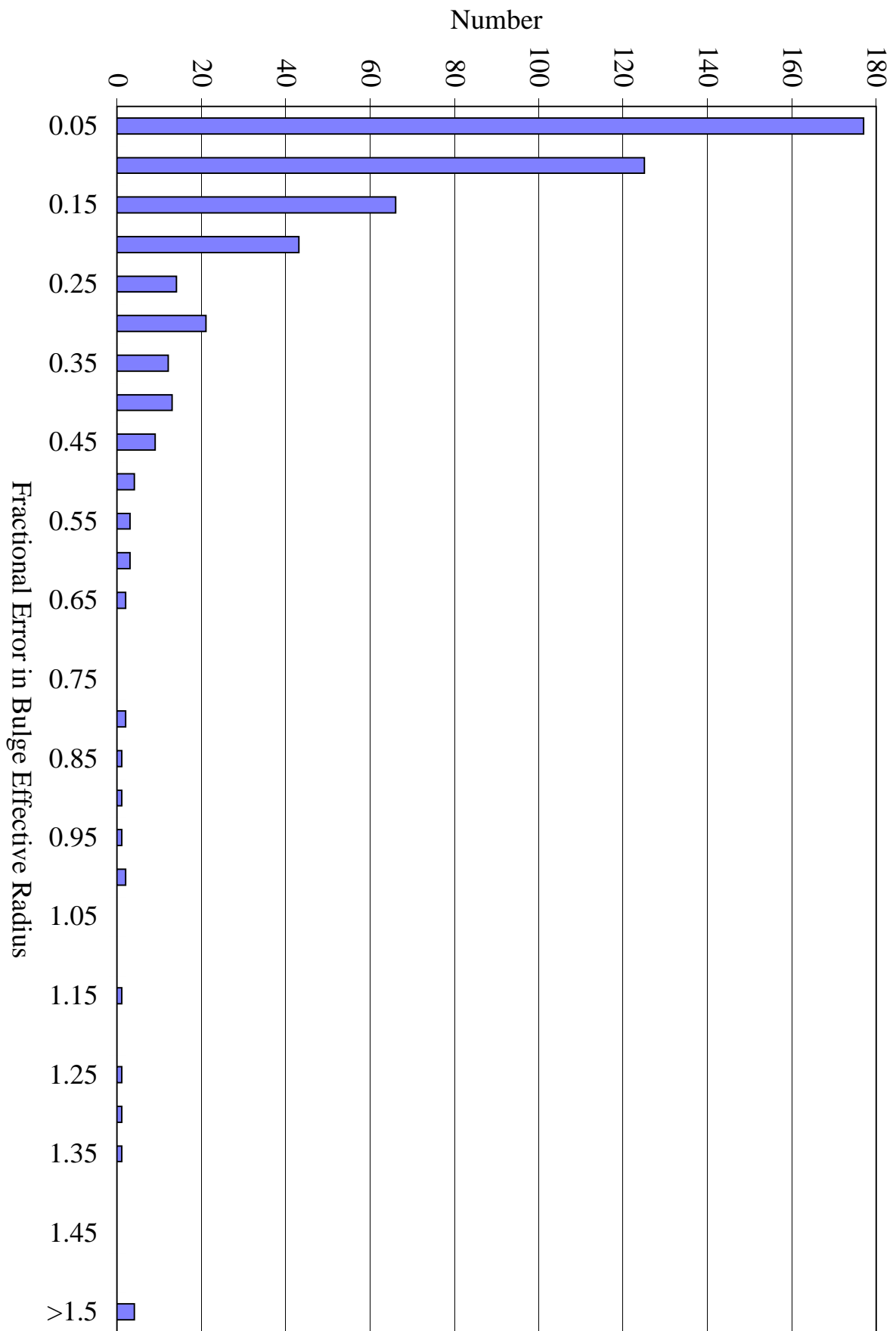
Col. 3 – Fractional error in  $r_e$

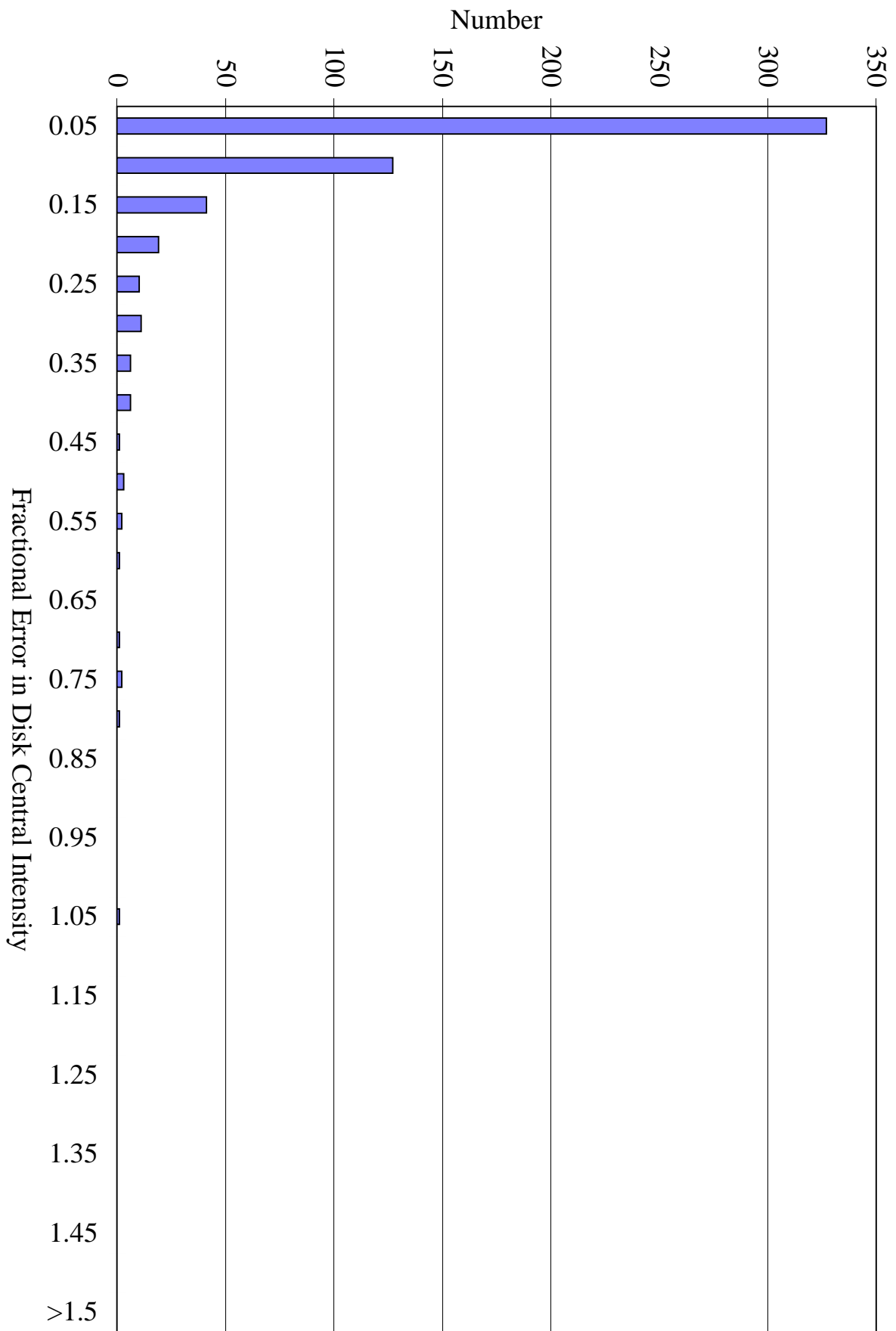
Col. 4 – Fractional error in  $I_0$

Col. 5 – Fractional error in  $r_0$

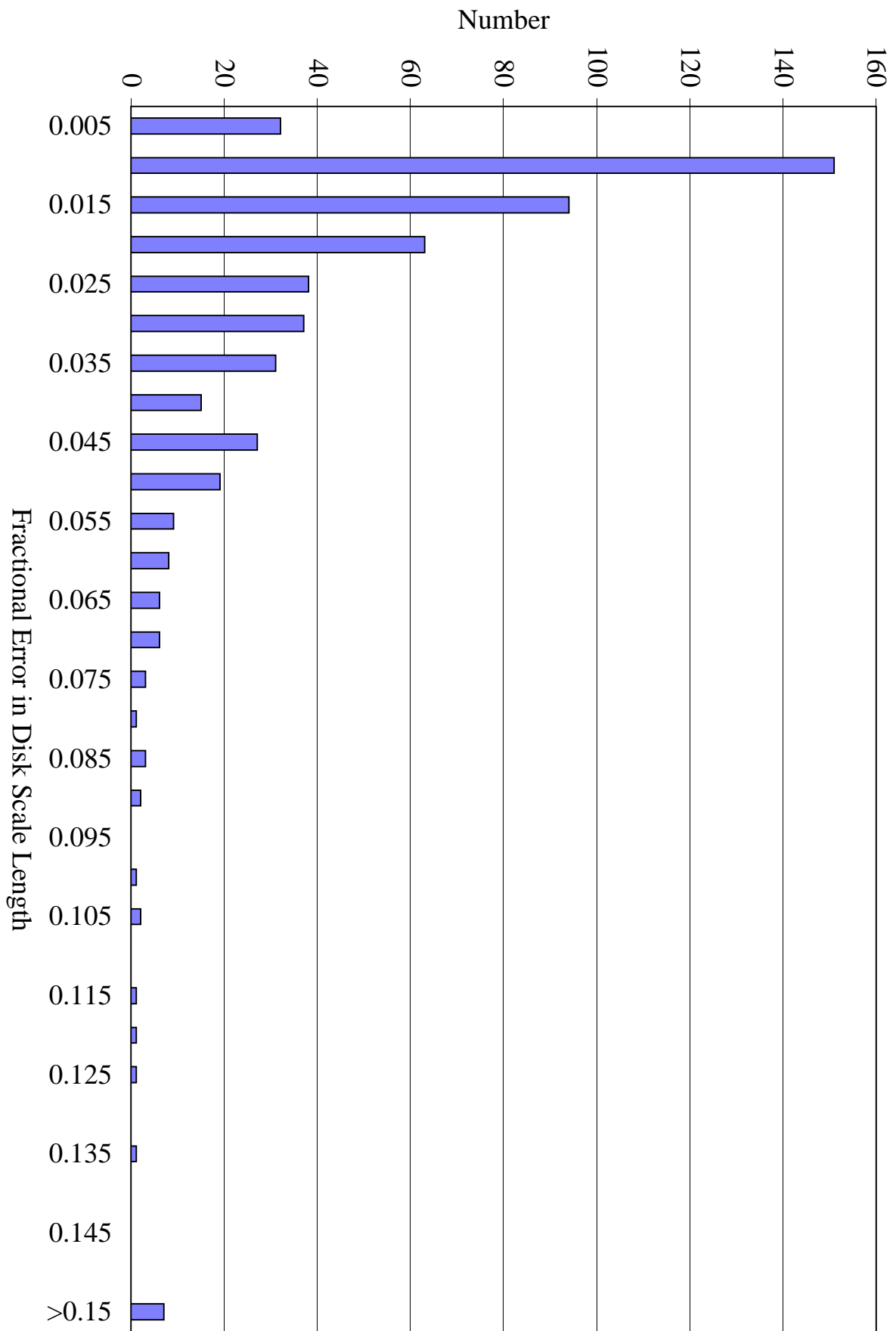
Col. 6 – Fractional error in  $r_h$











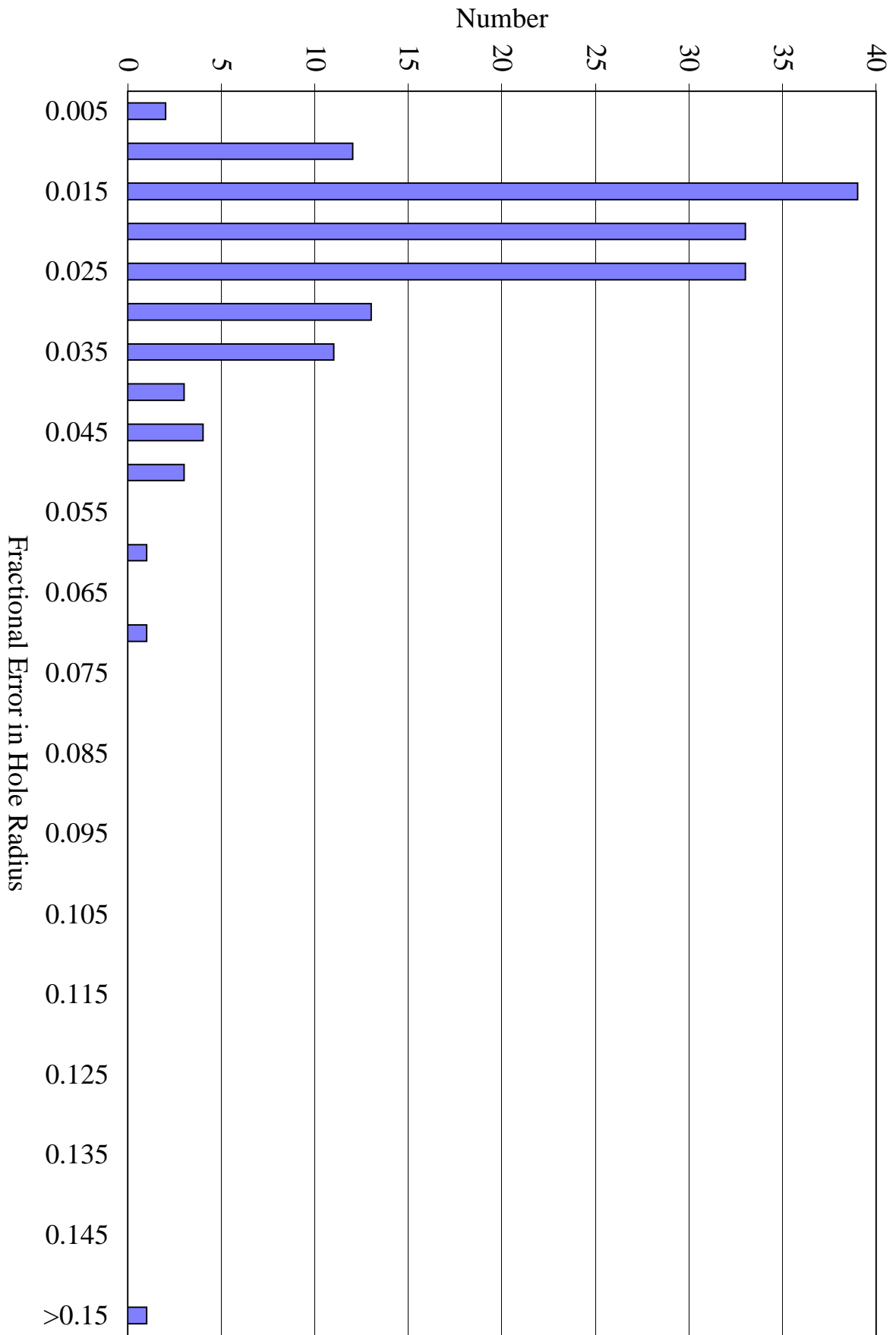


TABLE 4. Fractional Error Summary

Param	Num	Mean	Std.Dev.	Median	Min	Max
All fitted galaxies –						
$I_e$	507	43.2	912.3	0.126	0.014	20508.
$r_e$	507	0.194	0.910	0.082	0.010	19.4
$I_0$	559	0.075	0.110	0.040	0.000	1.03
$r_0$	559	1.67	38.8	0.016	0.003	917.9
$r_h$	156	0.022	0.015	0.019	0.005	0.160
The most discrepant galaxy removed –						
$I_e$	506	2.79	55.2	0.125	0.014	1241.3
$r_e$	506	0.156	0.317	0.082	0.010	5.0
$I_0$	558	0.073	0.102	0.040	0.000	0.767
$r_0$	558	0.027	0.064	0.016	0.003	1.304
$r_h$	155	0.021	0.010	0.019	0.005	0.068

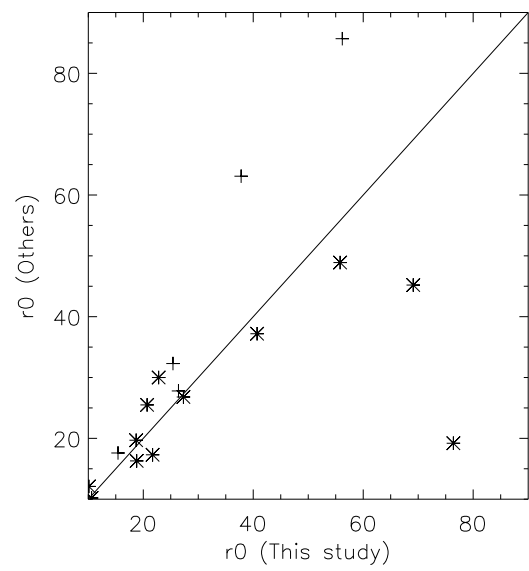
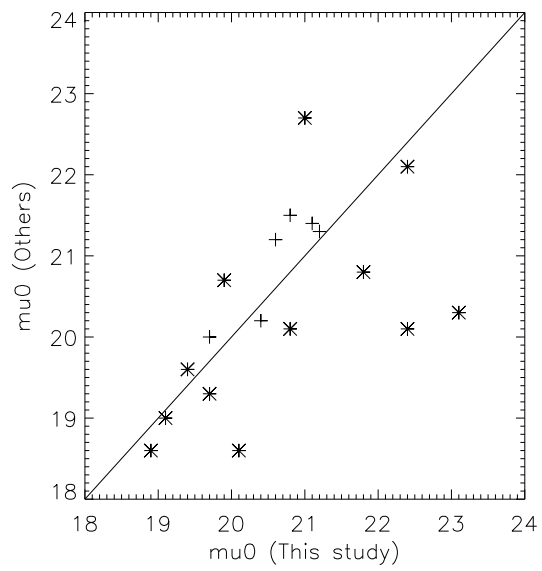
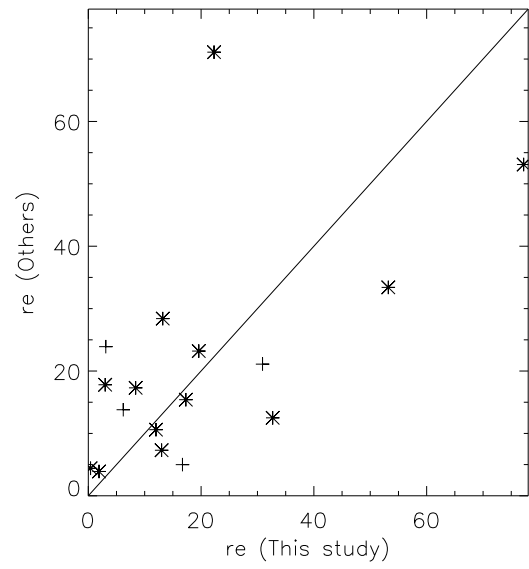
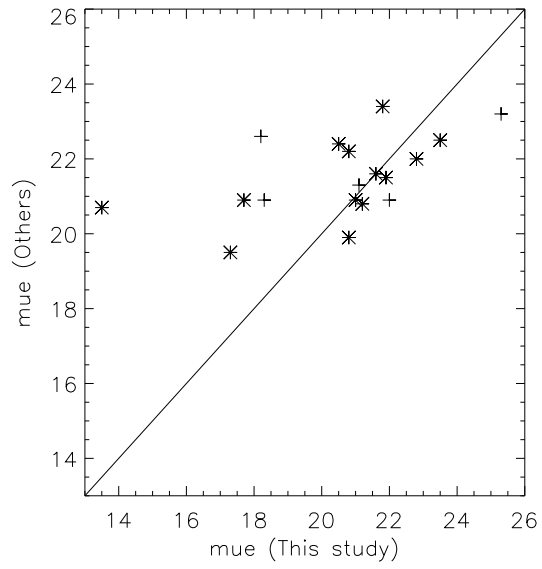


TABLE 5. Fitting Comparisons

Galaxy	P.D.( $I_e$ )	P.D.( $r_e$ )	P.D.( $I_0$ )	P.D.( $r_0$ )	Ref.
N0016	80%	-56%	159%	-14%	Kent (1985)
N0628	146%	-169%	-8%	42%	Boroson (1981)
N0670	35%	-11%	-12%	18%	Kent (1985)
N2268	88%	-108%	25%	5%	Boroson (1981)
N2639	-114%	73%	11%	-4%	Kent (1985)
N2683	-125%	105%	30%	-13%	Kent (1985)
N2776	87%	-89%	55%	5%	Kent (1985)
N2782	8%	-13%	171%	-120%	Kent (1985)
N2880	-180%	142%	-135%	27%	Kent (1985)
N3627	41%	-46%	118%	-42%	Kent (1985)
N3898	-168%	76%	-65%	50%	Boroson (1981)
N5380	-154%	69%	82%	-23%	Kent (1985)
N5533	0%	17%	34%	-9%	Kent (1985)
N5676	-200%	167%	43%	-2%	Kent (1985)
N5970	-142%	69%	-2%	21%	Kent (1985)
N6340	-193%	154%	-53%	24%	Boroson (1981)
N7331	-23%	-49%	-30%	16%	Boroson (1981)
Boroson (1981), Kent (1985) comparison:					
N0488	112%	-127%	-12%	-7%	
N2967	195%	-180%	-37%	11%	

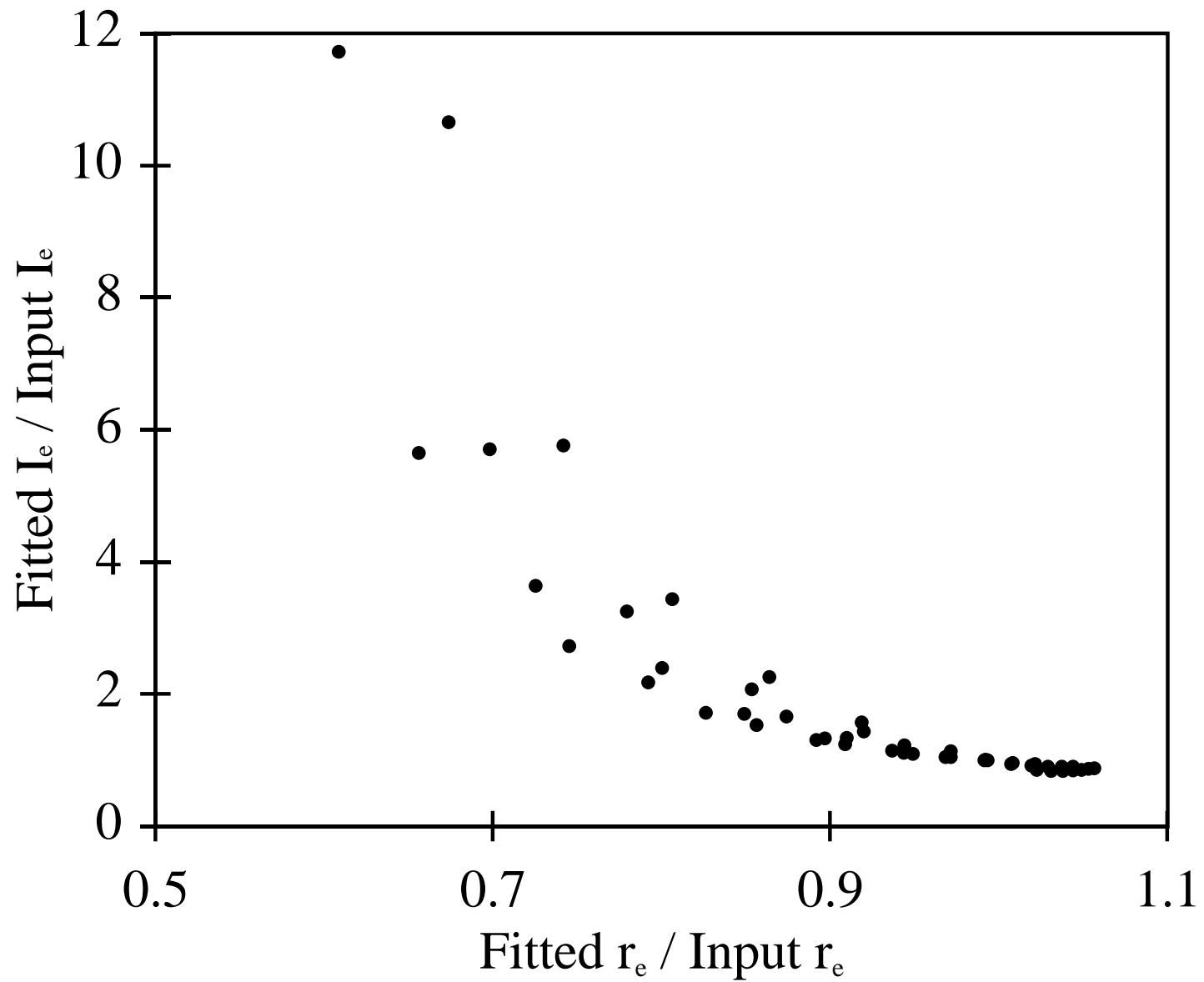
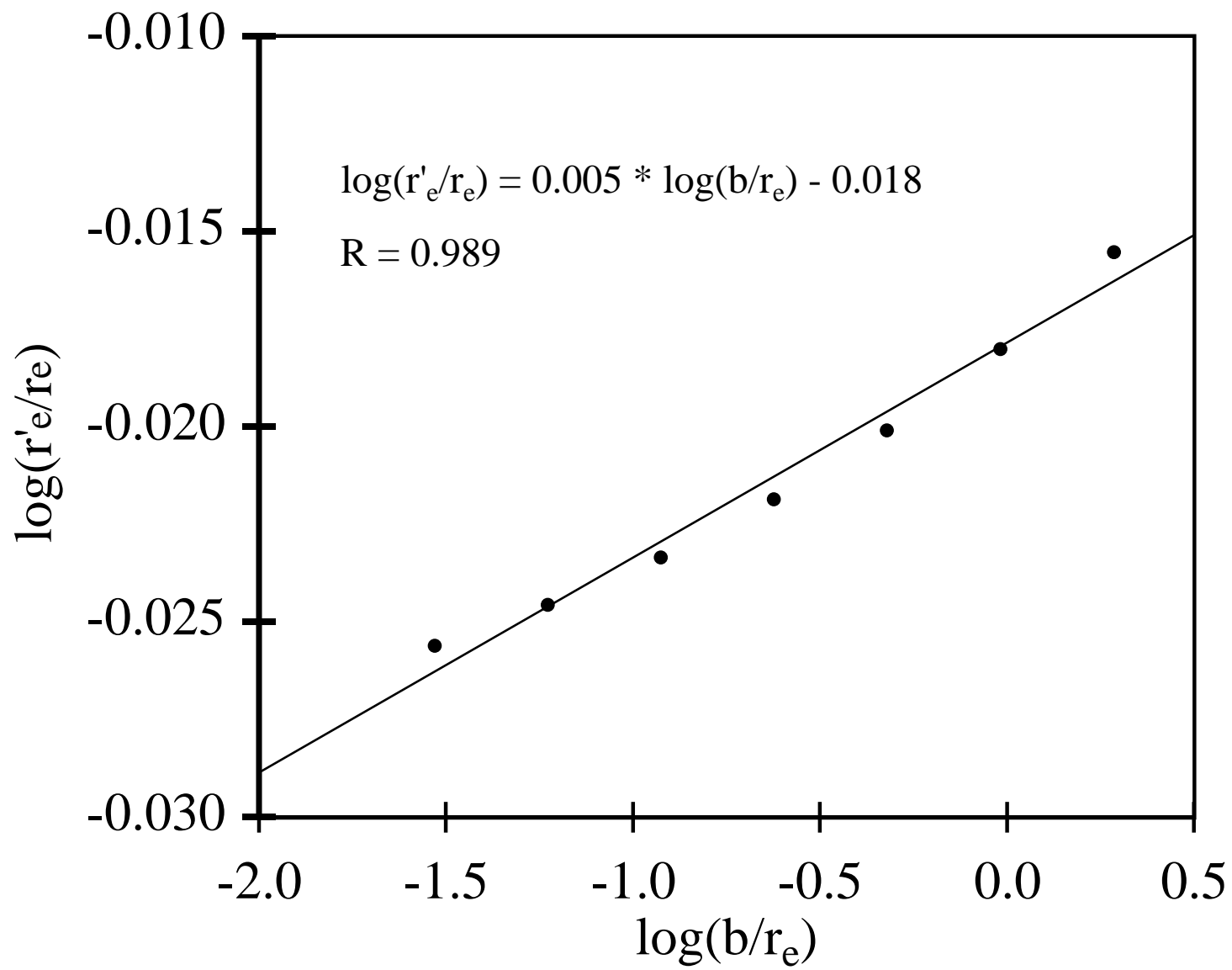


TABLE 6. Median Fractional Error Morphology Dependence

T-Type Range	$\Delta(I_e)$	$\Delta(r_e)$	$\Delta(I_0)$	$\Delta(r_0)$	$\Delta(r_h)$
$-3.5 \leq T < -0.5$	0.09 (131)	0.05 (131)	0.06 (119)	0.03 (119)	0.02 (41)
$-0.5 \leq T < 2.5$	0.12 (114)	0.07 (114)	0.05 (100)	0.02 (100)	0.02 (27)
$2.5 \leq T < 5.5$	0.14 (204)	0.10 (204)	0.03 (246)	0.01 (246)	0.02 (71)
$5.5 \leq T < 9.5$	0.24 (58)	0.17 (58)	0.02 (94)	0.01 (94)	0.02 (17)

The numbers in parentheses are the number of galaxies contributing to the median fractional error.





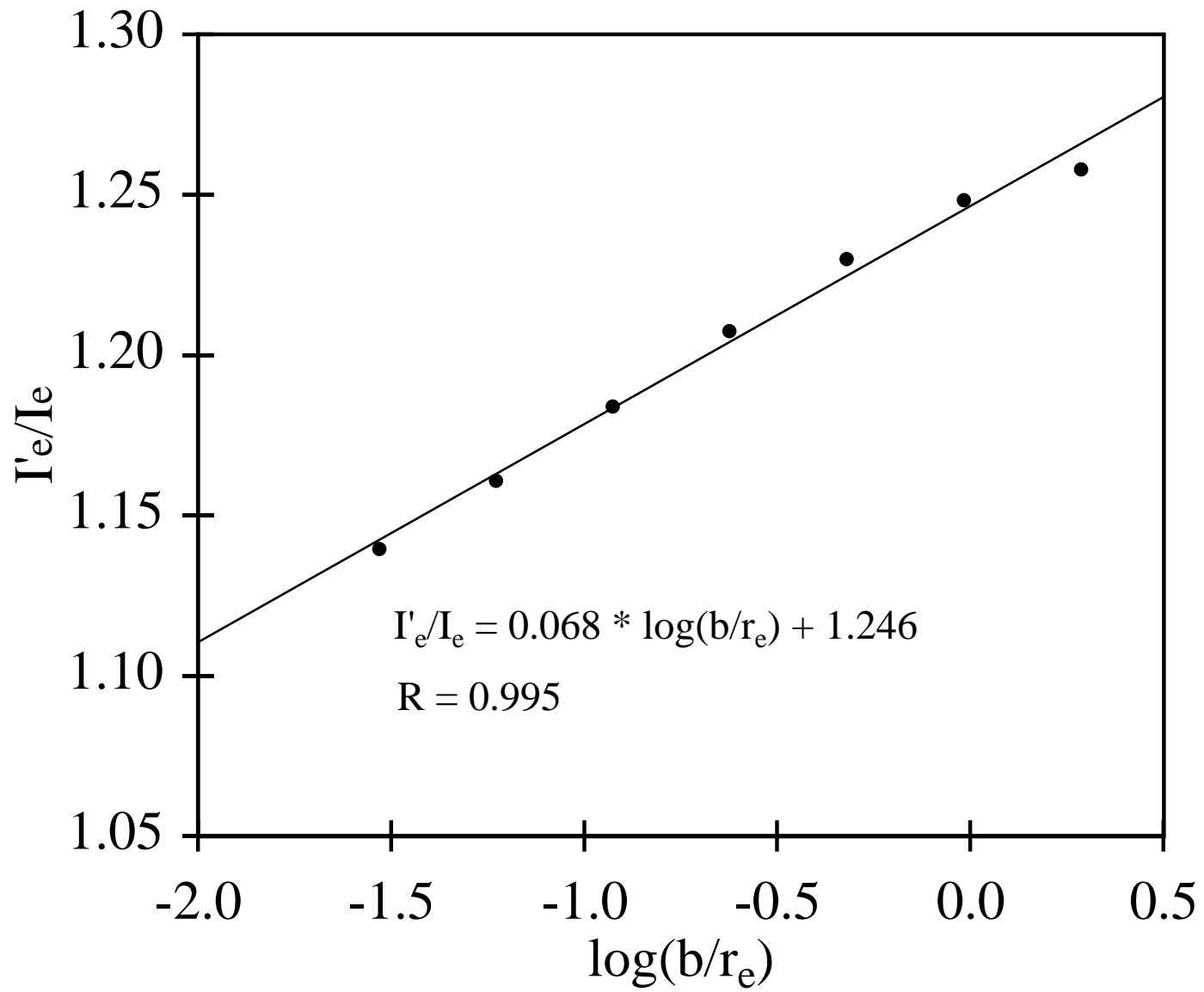


TABLE 7. Median Fractional Error Bar Class Dependence

Bar Class	$\Delta(I_e)$	$\Delta(r_e)$	$\Delta(I_0)$	$\Delta(r_0)$	$\Delta(r_h)$
SA	0.11 (173)	0.08 (173)	0.04 (173)	0.02 (173)	0.02 (42)
SB	0.12 (154)	0.08 (154)	0.05 (176)	0.02 (176)	0.02 (61)
SX	0.16 (148)	0.09 (148)	0.04 (170)	0.01 (170)	0.02 (44)
Not Typed	0.16 (32)	0.07 (32)	0.03 (40)	0.01 (40)	0.02 (9)

The numbers in parentheses are the number of galaxies contributing to the median fractional error.

TABLE 8. Median Fractional Error Inclination Dependence

Error	$i \leq 30^\circ$	$30^\circ < i \leq 60^\circ$	$i > 60^\circ$
$\Delta(I_e)$	0.12 (68)	0.12 (291)	0.14 (148)
$\Delta(r_e)$	0.09 (68)	0.08 (291)	0.09 (148)
$\Delta(I_0)$	0.05 (76)	0.05 (283)	0.02 (200)
$\Delta(r_0)$	0.02 (76)	0.02 (283)	0.01 (200)
$\Delta(r_h)$	0.02 (24)	0.02 (92)	0.02 (40)

The numbers in parentheses are the number of galaxies contributing to the median fractional error.

TABLE 9. Model Profile Fitting Results (*Input*  $I_e = 1000$ )

<i>Input</i> $r_e$ (")	<i>Fitted</i> $r_e$ (")	$\frac{\textit{Fitted } r_e}{\textit{Input } r_e}$	<i>Fitted</i> $I_e$	$\frac{\textit{Fitted } I_e}{\textit{Input } I_e}$
Seeing=1":				
0.5	0.51	1.02	856.7	0.86
1.0	1.03	1.03	843.6	0.84
2.0	2.08	1.04	842.3	0.84
4.0	4.18	1.04	848.4	0.85
8.0	8.39	1.05	858.7	0.86
16.0	16.85	1.05	871.1	0.87
32.0	33.81	1.06	884.2	0.88
Seeing=2":				
0.5	0.49	0.97	1139.2	1.14
1.0	0.99	0.99	1009.4	1.01
2.0	2.01	1.01	947.8	0.95
4.0	4.08	1.02	917.9	0.92
8.0	8.23	1.03	905.2	0.91
16.0	16.60	1.04	902.4	0.90
32.0	33.41	1.04	905.2	0.91
Seeing=3":				
0.5	0.46	0.92	1571.1	1.57
1.0	0.92	0.92	1437.7	1.44
2.0	1.89	0.94	1223.8	1.22
4.0	3.88	0.97	1080.4	1.08
8.0	7.93	0.99	1004.0	1.00
16.0	16.13	1.01	964.7	0.96
32.0	32.69	1.02	945.2	0.95
Seeing=4":				
0.5	0.43	0.86	2260.0	2.26
1.0	0.85	0.85	2071.9	2.07
2.0	1.75	0.87	1665.8	1.67
4.0	3.64	0.91	1340.2	1.34
8.0	7.55	0.94	1153.8	1.15
16.0	15.54	0.97	1053.2	1.05
32.0	31.79	0.99	998.8	1.00
Seeing=5":				
0.5	0.40	0.81	3440.4	3.44
1.0	0.78	0.78	3254.8	3.25
2.0	1.60	0.80	2396.8	2.40
4.0	3.40	0.85	1700.3	1.70
8.0	7.18	0.90	1336.4	1.34
16.0	14.99	0.94	1150.6	1.15
32.0	30.99	0.97	1052.4	1.05

TABLE 9. (continued)

<i>Input <math>r_e</math> (")</i>	<i>Fitted <math>r_e</math> (")</i>	<i><math>\frac{Fitted r_e}{Input r_e}</math></i>	<i>Fitted <math>I_e</math></i>	<i><math>\frac{Fitted I_e}{Input I_e}</math></i>
Seeing=6":				
0.5	0.37	0.74	5767.5	5.77
1.0	0.70	0.70	5709.5	5.71
2.0	1.45	0.73	3641.8	3.64
4.0	3.17	0.79	2176.4	2.18
8.0	6.85	0.86	1534.6	1.53
16.0	14.54	0.91	1241.8	1.24
32.0	30.37	0.95	1100.2	1.10
Seeing=7":				
0.5	0.34	0.67	10658.8	10.66
1.0	0.61	0.61	11727.6	11.73
2.0	1.31	0.66	5652.2	5.65
4.0	2.98	0.75	2726.0	2.73
8.0	6.61	0.83	1716.7	1.72
16.0	14.27	0.89	1308.3	1.31
32.0	30.19	0.94	1117.8	1.12

TABLE 10. Interpolation Data for Seeing Correction

$S''$	$S/r'_e$	$I_e^0/I'_e$	$r_e^0/r'_e$	$S''$	$S/r'_e$	$I_e^0/I'_e$	$r_e^0/r'_e$
1	2.03	0.922	1.015	5	12.857	0.228	1.286
1	1.011	0.952	1.011	5	6.675	0.245	1.335
1	0.504	0.969	1.008	5	3.263	0.339	1.305
1	0.251	0.979	1.006	5	1.544	0.486	1.235
1	0.126	0.984	1.005	5	0.734	0.63	1.174
1	0.063	0.987	1.005	5	0.353	0.745	1.129
1	0.031	0.99	1.005	5	0.171	0.83	1.096
2	4.274	0.692	1.068	6	16.764	0.136	1.397
2	2.101	0.795	1.05	6	8.938	0.139	1.49
2	1.038	0.861	1.038	6	4.319	0.222	1.44
2	0.515	0.904	1.03	6	1.986	0.379	1.324
2	0.256	0.933	1.024	6	0.922	0.548	1.23
2	0.128	0.953	1.02	6	0.436	0.69	1.164
2	0.064	0.967	1.017	6	0.21	0.793	1.119
3	6.777	0.501	1.129	7	21.527	0.073	1.538
3	3.396	0.557	1.132	7	11.954	0.068	1.708
3	1.662	0.666	1.108	7	5.567	0.143	1.591
3	0.811	0.767	1.082	7	2.461	0.302	1.407
3	0.399	0.84	1.063	7	1.115	0.489	1.274
3	0.197	0.89	1.049	7	0.519	0.654	1.186
3	0.097	0.925	1.04	7	0.246	0.781	1.125
4	9.606	0.348	1.201				
4	4.879	0.386	1.22				
4	2.391	0.488	1.196				
4	1.153	0.618	1.153				
4	0.558	0.73	1.116				
4	0.272	0.815	1.089				
4	0.134	0.875	1.069				

## Bulge-Disk Decomposition of 659 Spiral and Lenticular Galaxy Brightness Profiles

W. E. Baggett

Science Programs, Computer Sciences Corporation  
3700 San Martin Drive, Baltimore, MD 21218  
baggett@stsci.edu

S. M. Baggett

Space Telescope Science Institute  
3700 San Martin Drive, Baltimore, MD 21218  
sbaggett@stsci.edu

K. S. J. Anderson

Department of Astronomy, New Mexico State University,  
P. O. Box 30001, Dept. 4500, Las Cruces, NM 88003  
kurt@nmsu.edu

### ABSTRACT

We present one of the largest homogeneous sets of spiral and lenticular galaxy brightness profile decompositions completed to date. The 659 galaxies in our sample have been fitted with a deVaucouleurs' law for the bulge component and an inner-truncated exponential for the disk component. Of the 659 galaxies in the sample, 620 were successfully fit with the chosen fitting functions. The fits are generally well-defined, with more than 90% having RMS deviations from the observed profile of less than 0.35 magnitudes. We find no correlations of fitting quality, as measured by these RMS residuals, with either morphological type or inclination. Similarly, the estimated errors of the fitted coefficients show no significant trends with type or inclination.

These decompositions form a useful basis for the study of the light distributions of spiral and lenticular galaxies. The object base is sufficiently large that well-defined samples of galaxies can be selected from it.

*Subject headings:* galaxies: spiral — galaxies: photometry

## 1. Introduction

In order to compare the large-scale characteristics of galaxies objectively, quantitative measures of the structural components are necessary. There are many schemes for describing the structure of galaxies, including Hubble classification (Sandage, 1961), isophotal radii (Holmberg, 1947), concentration parameters (Kent, 1985; Kodaira et al., 1990), and the use of various fitting functions (deVaucouleurs, 1953; Freeman, 1970; Kormendy, 1977). All these techniques specify parameters which can provide insight into the formation and evolution of galaxies. The use of standardized fitting functions is arguably the most powerful method for measuring the large-scale structure of galaxies, as the functions yield a variety of parameters which can be easily compared with the results of theoretical models. They also provide a reasonably detailed description of the radial light distribution with a small number of parameters.

Ideally, fitting functions would be based upon the physics of the formation and evolutionary processes. Unfortunately, these processes are neither simple nor well-understood, so the most commonly used functions are derived empirically. Traditional fitting functions for elliptical galaxies and spiral galaxy bulges include the Hubble law (Hubble, 1930), King model (King, 1966), and deVaucouleurs law (deVaucouleurs, 1953). Recently, there has been some work which suggests that a generalized version of the deVaucouleurs profile ( $r^{1/n}$ ) provides for better bulge fits (Andredakis, Peletier, and Balcells, 1995), and that late-type spirals often have bulges which are best fitted by exponentials (Andredakis and Sanders, 1994). Exponentials (Freeman, 1970) and inner-truncated exponentials (Kormendy, 1977) work well for the disk components of spiral galaxies. Overall, the deVaucouleurs law seems to be quite effective as a fitting function for bulges; it can be written as

$$I_B(r) = I_e \times 10^{-3.33((r/r_e)^{1/4}-1)} \quad (1-1)$$

where  $I_B(r)$  is the surface intensity of the bulge at radius  $r$ ,  $r_e$  is a characteristic radius defined to be the radius within which half the total light is emitted, and  $I_e$ , the effective intensity, is simply the surface intensity at  $r_e$ . (In this paper, we will consistently use the term "surface intensity,"  $I$ , to mean linear intensity units per square arcsecond, and "surface brightness,"  $\mu$ , to mean the same quantity in magnitude units.) Similarly, the inner-truncated exponential is defined by Kormendy (1977) as

$$I_D(r) = I_0 \times \exp -(r/r_0 + (r_h/r)^n) \quad (1-2)$$

where  $I_D(r)$  is the disk surface intensity at radius  $r$ ,  $I_0$  is the central intensity of the disk,  $r_0$  is the disk scale length, and  $r_h$  is the radius of the central cutoff of the disk ("hole radius"); the pure exponential disk is the same as equation (1-2) with  $r_h = 0$ . Kormendy (1977) found that a value of  $n \sim 3$  in the truncation term works well, and we have adopted  $n = 3$  for all of the fits presented



here. Figure 1 illustrates the usefulness of including a truncation term in the fitting function, using NGC 3145 as an example.

Others have used these fitting functions to obtain the relevant structural parameters for spiral galaxies in order to compare galaxies of different types, luminosities, and environments. For example, Boroson (1981) fit brightness profiles for 26 non-barred spiral galaxies in order to determine how the bulge-to-disk ratios are related to the Hubble types, and to investigate the relationship between spiral and S0 (lenticular) galaxies. Kent (1985) performed a similar analysis using 105 intrinsically luminous galaxies of all types. Kormendy (1977) decomposed the brightness profiles of seven compact S0 galaxies and one "normal" galaxy to check Freeman's (1970) hypothesis of a constant central disk surface brightness. More recently, deJong (1996) investigated the Freeman (1970) result of a constant central surface brightness of disks, and some other relationships between the fitting parameters and the Hubble sequence, using  $B$ - and  $K$  - *band* brightness profiles of 86 face-on disk galaxies.

A relatively recent innovation is to fit a surface to the entire galaxy image (Byun and Freeman 1995) using the above fitting functions and also solving for the center and ellipticity of the projected distributions. A general advantage of this approach is that the bulge and disk components can be allowed to have different ellipticities, which alleviates the problem of projection effects for moderate- to high-inclination systems: because the rounder bulge is typically sampled at a smaller galactocentric radius than the inclined disk for a given position in the image, the derived bulge parameters are systematically too large when estimated from brightness profiles obtained by azimuthal averaging techniques. However, the profiles used here are major axis cuts (see below), so this difficulty should not affect our fitted parameters (Burstein 1979). The cost of using major axis cuts is that of throwing away much of the information in the images.

All of these programs except Kormendy (1977) employed a simple exponential to describe the disk light distribution. As part of a study of the origin of inner-truncated spiral galaxy disks, or Type II brightness profiles (Freeman, 1970), we have used the deVaucouleurs' law and the inner-truncated disk fitting function from Kormendy (1977) for the bulge-disk decomposition of 659 spiral and lenticular galaxy brightness profiles. Our preliminary study (Baggett, Baggett, and Anderson, 1993) indicated that a substantial fraction of all spiral galaxies exhibit an inner-truncation, so the inclusion of such a term in the fitting function seems justified with this large set of brightness profiles. Furthermore, the data set used in this study is extremely homogeneous, all images having been obtained, reduced, and analyzed in the same way. Thus, the results of our fitting should be a useful resource for many studies of the large-scale properties of disk galaxies. The following sections will describe the data and the bulge-disk decomposition procedures, and will present the fitting results together with a discussion of the associated errors.

## 2. Data

The brightness profiles used for this study were obtained from Kodaira et al. (1990; hereafter, PANBG) in a machine-readable form. The initial PANBG sample of galaxies was selected on the basis of being included in *A Revised Shapley-Ames Catalog of Bright Galaxies* (Sandage and Tammann, 1981; hereafter, RSA) and being north of declination  $-25^\circ$ . Of the 911 such galaxies in the RSA, 791 are included in the PANBG, and 659 of those have Hubble types (T-Types) from the *Third Reference Catalogue of Bright Galaxies* (deVaucouleurs et al., 1991; hereafter RC3) in the range -3 to 9, which indicates that they are spiral or lenticular galaxies. These 659 galaxies form the basis of our study.

Galaxies in the PANBG were observed photographically over a period of almost two decades (late 1970’s through 1988) with the Kiso Observatory 1.05-m Schmidt telescope, using Kodak IIa-D plates and a Schott GG495 glass filter to define the ”photographic V-band.” Exposure times ranged from 30 minutes to 60 minutes, with 50 minutes being standard, and the plates were developed in Fuji Pandol or Kodak D-19 developer. The plates were then digitized with the Kiso Observatory PDS microdensitometer utilizing a  $1''$  square aperture, except for NGC 224 and NGC 598, which were measured with a  $10''$  square aperture. Each plate included a step wedge image which was scanned in the same fashion as the galaxy images. Measured densities were converted into relative intensities via the wedge calibrator, and the aperture photometry from Longo and deVaucouleurs (1983) was then used to transform the resulting magnitudes to a standard photometric system. The stated internal photometric accuracy in the PANBG is about 0.1 magnitudes (standard deviation), and is dominated by errors in the absolute calibration.

The brightness profiles in the PANBG were obtained from the resulting calibrated images by taking a cut along the apparent major axis of each galaxy. The major axis was defined by fitting the  $25 V - mag \text{ arcsec}^{-2}$  isophote with an ellipse whose center was fixed at the center of gravity of a  $21 \times 21$  pixel region around the apparent nucleus of the galaxy. The surface brightness was then sampled along this axis using a circular aperture which was stepped outward from the galaxy center in 2-pixel steps ( $2''$  for all but NGC 224 and NGC 598, which used  $20''$  steps). The aperture used was 2 pixels in diameter at the galaxy center and the diameter was varied in such a way as to be tangent to a sector with a 5 degree vertex angle centered on the major axis. This scheme of varying the aperture size was chosen in order to compensate for the decreased signal-to-noise ratio in the outer portions of the galaxies. As a result, there is some radial smearing of the intensity information at large galactocentric radii, smoothing structure in the outer portions of each profile. Further smoothing results from our averaging of the two halves of the major axis cut to produce the final profiles. For full details of the data acquisition and reduction processes, the reader is referred to PANBG.

### 3. Fitting

#### 3.1. Procedure

The major axis brightness profiles were fitted using a combination of a deVaucouleurs’ (1953) law (equation 1-1) and an inner-truncated exponential (Kormendy, 1977; equation 1-2). The interactive STSDAS task ‘nfit1d’ was used for all of the fitting; this task uses the downhill simplex algorithm for performing a non-linear least-squares fit of the data to a specified function, and allows interactive control over the inclusion of the various parameters and the range of the data to be fit. It is a very flexible routine and we found that it accurately returns the values of the fitting parameters in a number of test cases. Fitting is performed on the surface intensity data and is accomplished by minimizing the weighted RMS deviation of the data from the fit.

The most appropriate weighting function,  $w_i$ , is one which uses the variance of the intensity measurement for each point as its basis, with the weight of the  $i^{th}$  point being

$$w_i = \frac{1}{\sigma_i^2} \tag{3-1}$$

where  $\sigma_i^2$  is the variance of the  $i^{th}$  point (Bevington, 1969). We chose to use a weighting based on the Poisson distribution, where  $\sigma_i \propto \sqrt{I}$ , as this was consistent with the fashion in which the intensity measurements were obtained.

An unfortunate side effect of this  $1/I_i$  weighting function is that it destroys the usefulness of the weighted RMS residual as a goodness of fit measure *between* galaxies. The value of the weighted RMS residual is highly dependent upon the fitting range, with fits to lower surface intensities being virtually guaranteed a lower weighted RMS value than fits stopping at higher surface intensities. As a result, the weighted RMS residual is a useful diagnostic only during the fitting process for a given galaxy and, as such, the weighted RMS values for each fit are not reported here.

However, the *unweighted* RMS residuals,  $\sqrt{[\sum(\mu_i - \mu_{fit})^2]/N}$ , can be computed after the fact, and we have tabulated these values, expressed in magnitude units, as a basis for assessing the relative quality of the fits. These residuals were computed from the portions of each brightness profile at radii larger than  $3''$  and out to the point where the profile first drops to a surface brightness fainter than  $25 V - mag \text{ arcsec}^{-2}$ . Hence, all of the calculations avoid the portion of the profile most affected by seeing, and reach the same limiting surface brightness. Also, any structure present in the profile contributes to this measure, and thus galaxies with significant structure will be recognizable by their correspondingly larger RMS value. In this way, the unweighted RMS residuals are directly comparable from galaxy to galaxy, and reflect more accurately the quality of the fits than do the weighted RMS residuals.

Aside from the weighting function, the only other controlled aspect of the fitting was the choice

of components to include in each fit. Generally, all fits were attempted with both a bulge and a pure exponential disk, resulting in the estimation of four quantities and their uncertainties:  $I_e$ ,  $r_e$ ,  $I_0$ , and  $r_0$ ; inner-truncated disks, with the additional parameter,  $r_h$ , were only utilized if the profile had the suggestion of a plateau near the center. If any component (bulge, disk, inner-truncated disk) was fit with a negative value for a coefficient, that component was deemed non-physical and was removed from the fitting function. In cases where the need for a specific component was not obvious, fits with and without it were obtained and the component was included if the *weighted* RMS value was smaller by at least 10% than the fit without the component.

A sample of the results of the fitting are presented in Table 1, which provides for each galaxy its NGC/IC designation (as indicated by a leading "N" or "I", respectively), its revised Hubble type, T-type, and axis ratio from the RC3, and the fit parameters determined here. The fit parameters are given as the fitting range in arcseconds (in the format minimum:maximum), the bulge effective surface brightness ( $\mu_e$ ), the bulge effective radius ( $r_e$ ), the disk central surface brightness ( $\mu_0$ ), the disk scale length ( $r_0$ ), and the disk hole radius ( $r_h$ ). The table also includes the seeing as reported in the PANBG, and the seeing-corrected values of the fitted bulge parameters ( $\mu_e^0$  and  $r_e^0$ ; see the Appendix). The last two columns contain the unweighted RMS deviation of the fit from the profile in  $V - mag \text{ arcsec}^{-2}$  and a column of notes. All surface brightness quantities are in units of  $V - mag \text{ arcsec}^{-2}$ , and all radii are in units of arcseconds. No corrections for galactic extinction, internal extinction, or inclination have been applied — the fits are for the observed major axis profile. We have chosen to present the results for the observed profiles in order to allow the reader the opportunity to apply the corrections (s)he deems most appropriate; we therefore avoid the necessity of uncorrecting our fits and subsequently applying a different correction.

The fitting procedure did not include any allowance for the effects of seeing on the brightness profile. In the Appendix, we describe an experiment which was designed to quantify the impact on the fitted bulge parameters of excluding seeing from the fitting; the net result is that our fitted  $I_e$  tends to be too large by up to an order of magnitude when the seeing is much larger than the input effective radius, and our fitted  $r_e$  tend to be slightly too small in the same cases. This is what is intuitively expected, of course.

Although the profile definition procedure introduces a significant level of radial smearing, structure is still apparent in many of the profiles. The fitting process nominally made no allowance for the presence of structure, fitting across arms and bars as if they were simply noise in the data, except in some specific instances. These instances occur when a very strong, isolated feature is present — then the radial range occupied by the feature was excluded from the fit. If a strong feature is present at the end of the fitting range, the fitting range was suitably shortened. The existence of such a condition was manually determined, and is indicated in Table 1 by the presence of multiple ranges in the fitting range column and/or by a note ("A") in the last column of the table.

Figure 2 presents the profiles and fits for the galaxies from Table 1. Each plot shows the observed profile from the PANBG as crosses, and the fitted bulge and disk components and their sum as solid lines. In addition, the range of radius included in the fit is indicated by the horizontal line(s) at the  $25.3 V - mag \text{ arcsec}^{-2}$  level, and the fit parameters are provided near the top of each plot. This selection of objects includes some very good fits as measured by the RMS deviations (NGC 0016, NGC 0404), some typical-quality fits (NGC 0224, NGC 0237), some fits which avoid strong structure in the profile (NGC 0151, NGC 0157, NGC 0253), and one of the worst fits in the entire sample (NGC 0289).

There were 39 galaxies in the sample for which no fits were obtained; these objects are listed in Table 2, with their revised types and axis ratios from the RC3. These galaxies are particularly ill-suited for fitting by the selected fitting functions, as many of them have pronounced concavities toward low surface brightness or multiple exponential components in their brightness profiles – the chosen functions simply do not represent their light distributions in any meaningful way.

Finally, there are also several fits (e.g., NGC 0016, NGC 0628, NGC 0890, and NGC 5033) where the disk component is everywhere fainter than the bulge, and other fits where the disk becomes brighter than the bulge only at intermediate radii (e.g., NGC 0670, NGC 0955, NGC 1090, and NGC 1187). In both of these situations, the bulge fit might have benefitted from an alternative functional form, perhaps the generalized deVaucouleurs’ law as discussed by Andredakis, Peletier, and Balcells (1995), although no attempt has been made to investigate this in the present study.

### 3.2. Fitting Errors

We have chosen three methods of estimating the fitting errors: 1) unweighted RMS residuals, 2) error estimates provided by the fitting software, and 3) comparison with the results of other workers.

The unweighted RMS residuals for each fit are tabulated in Table 1. Because we have computed them in a uniform fashion for all objects, including all structure in the profiles, these values provide an unbiased and consistent measurement of how well the fitting functions and the determined parameters describe the observed brightness distribution. From these values we find that the median RMS deviation of the fits is only 0.15 mag, and that more than 90% of the fits are better than 0.35 mag; Figure 3 shows the distribution of the RMS deviations using bins of width 0.05 magnitude. The overall ability of the fits to describe the brightness distributions is quite good, given that the unweighted RMS residuals include all of the structure present in the profile.

In an effort to quantify the value of the unweighted residuals as a measure of the goodness of fit, we have examined plots of the profiles and selected the best examples of profiles without significant structure and which appear to be well represented by the chosen fitting functions. Note that this selection did not involve consideration of the computed unweighted RMS residuals. There were 16 objects included in this selection, and they have a mean unweighted RMS deviation

of 0.05 magnitudes and a range of 0.03 magnitudes to 0.10 magnitudes; this suggests that fits with unweighted RMS residuals greater than about 0.10 magnitudes are affected to some degree by significant structure and/or poor fitting quality. The full sample contains 161 galaxies with RMS residuals of 0.10 magnitudes or less.

At the other end of the distribution, the worst-fit galaxies have been investigated to attempt to find out why they were so poorly fit. We have inspected the 18 galaxies which have unweighted RMS residuals greater than 0.5 magnitudes to search for common characteristics such as morphology and inclination. The T-Type distribution of these 18 galaxies is essentially the same as for the sample as a whole, so there appears to be no correlation between poor fit and T-Type. There also appears to be no serious trend with inclination: the mean inclination of the group is  $57^\circ$ , consistent with a random distribution of tilts. The most common characteristic is a low-surface brightness extension to the brightness profile, such that the fit falls below the measurements in the outer portion. The extension is sometimes featureless, sometimes it contains a distinct bump (as if an outer ring or arm); sometimes it is nearly constant brightness and other times it is more or less parallel with the inner profile. There is only one case (NGC 0157) where the problem region is in the main portion of the disk, and this galaxy looks disturbed, almost as if undergoing a collision. The apparent overriding reason for the poor fits is simply that the chosen fitting functions do not work well for some galaxies. This same conclusion holds for the 39 galaxies which were not fitted in this effort: common characteristics of these objects are extremely strong, large-scale structures, concavity of the brightness profile toward faint surface brightness, and apparent multiple components of the profile, usually with more than one exponential. This occasional inappropriateness of the fitting functions suggests that careful consideration of the fitted parameters and their error estimates should be exercised before judging whether a specific fit is truly meaningful for a detailed study of any individual galaxy.

The second method of judging the fitting errors was the use of estimated coefficient errors as produced by the fitting software. The 'nfit1d' task estimates the errors in each parameter by a process of bootstrap resampling, with a choice of distribution functions for use in the procedure. We used the Poisson distribution as the distribution function for the parameter error estimation as this reflects the photon statistics expected to affect the measured relative intensities in the brightness profiles. In order to minimize the effects of comparing parameters which vary wildly in value from galaxy to galaxy, we have computed the fractional error in each fitted parameter. Table 3 lists these fractional error estimates for a sample of the galaxies — column 1 gives the galaxy identification and columns 2 through 6 the fractional error of each of the parameters. Note that since the fitting was performed in the surface intensity scale (not surface brightness), the relative errors are computed in linear units, not magnitude units.

The fractional errors for the full set of galaxies are summarized in Table 4, which gives for each parameter the number of error estimates, the mean fractional error, the standard deviation of the fractional errors, the median fractional error, and the minimum and maximum fractional errors. As can be seen in Table 4, every parameter *except*  $I_0$  is significantly affected by outliers;

histograms of the fractional error of each parameter are shown in Figure 4, which demonstrate this problem. Removing the most discrepant outlier from the statistical calculations (second part of Table 4) improves the results considerably. Unfortunately, there is not just one "bad" fit in the sample causing all of these outlying points: the bulge parameter errors are both dominated by the fit for NGC 2441, while the disk central surface intensity error is affected by the fit for NGC 2541, the disk scale length error by NGC 5033, and the hole radius error by NGC 2997.

The bulge component of NGC 2441 dominates the disk only at radii smaller than about 6 arcsec, so there are very few data points defining the bulge and the coefficient uncertainties reflect this fact. The profile for NGC 2541 is fitted with a faint inner-truncated disk (the peak disk brightness is only about  $24 V - mag \text{ arcsec}^{-2}$ ) and the hole radius is more than six disk scale lengths from the galaxy center. The southern half of the brightness profile contains a relatively bright spiral arm (about  $23 V - mag \text{ arcsec}^{-2}$  at its brightest), and this asymmetry results in a bump in the averaged profile which has been fitted with the inner-truncation. NGC 5033 was fitted with a very faint ( $\mu_0 = 25.1 V - mag \text{ arcsec}^{-2}$ ), very flat disk ( $r_0 = 732 \text{ arcsec}$ ) which was never comparable in brightness to the bulge. As a result, the disk parameters for this galaxy are not well constrained by the data, and the estimated errors in the coefficients are correspondingly large. Finally, NGC 2997 has been fitted with a hole radius just smaller than the radius of the innermost data point point, so the value of the hole radius is, again, not really constrained by the data.

Because of the presence of these extreme outliers, the median fractional errors are much more useful than the mean for examining the fitting errors of the sample as a whole. The summary in Table 4 shows that the median coefficient fractional errors range from a low of 1.6% for the disk scale length to more than 12% for the bulge effective intensity. From these data, it is clear that the bulge parameters are the least well determined quantities in the fits, while the disk parameters are generally well determined. This is not unexpected: since the bulge coefficients are usually dominated by a relatively small number of data points, the constraints on them are not very strong.

Finally, a few of the galaxies included in this study have been previously fitted by others with the same fitting functions, providing a completely independent check of the results of our fitting procedure. There are five galaxies in the current study which are also included in Boroson (1981), and 12 are in common with Kent (1985), making a total of 17 measurements available for use in this comparison. Prior to making any comparisons between the various works, the surface brightness parameters reported in Boroson (1981) and Kent (1985) have been "uncorrected" for the effects of inclination and galactic absorption as applied in each study, and the length parameters have been converted from kiloparsecs to arcseconds using the distances adopted by those authors. Furthermore, Boroson (1981) lists values for the disk  $B - V$  color, which have been used to convert his disk central surface brightnesses from the B bandpass to the V. Finally, there are two galaxies in common between Boroson (1981) and Kent (1985), and the same analysis has been applied to them. The percentage differences between the fitting parameters from these

works and the present study have been computed and tabulated in Table 5. In this table, we list for each galaxy the percentage difference between the parameters in the referenced work and this study, and also between the two reference works; the last column identifies the reference work. The differences were computed in the sense reference work minus this study, and Boroson minus Kent. These data are also presented in Figure 5, which shows the fitting parameters from Boroson (1981) and Kent (1985) plotted against the values obtained in the present study.

In general, the fits from the various studies do not agree very well, although the disk fits are typically more similar than the bulge fits. The mean of the absolute values of the percentage differences are 105% for  $I_e$ , 83% for  $r_e$ , 61% for  $I_0$ , and 26% for  $r_0$ , with 17 objects for all parameters. Our bulge fits agree somewhat better with those of Kent (1985), while our disk central surface brightnesses are closer to Boroson’s (1981) results – this reflects the conversion of Boroson’s surface brightnesses to the V-band. Interestingly, our values of  $r_0$  agree equally well, on average, with both reference works, leading us to believe that a 25% scatter in the disk scale length is to be expected under the circumstances of this comparison (differing bandpasses, .

The bulge fit differences are dominated by the effects of the profile acquisition procedures used in the different studies: this work used a wedge-shaped major axis cut, while Boroson (1981) and Kent (1985) used two variations on azimuthal averaging. In particular, it has been pointed out by Boroson (1981) that azimuthally averaged profiles will be systematically too bright in the bulge-dominated regions due to sampling the rounder bulge at a smaller galactocentric radius than the disk, at a given position in the image. Inspection of Table 5 reveals that every instance of a large departure in  $I_e$  shows a large departure in  $r_e$  of the *opposite* sign. That our bulge parameters agree better with Kent (1985) than with Boroson (1981) probably reflects the use of fixed ellipticities and position angles by Boroson, while Kent allowed those quantities to vary with radius. As a result, the mean surface brightness around ellipses in bulge-dominated regions are more representative of the major axis with Kent’s profile acquisition procedure than with Boroson’s, hence the slightly better agreement with our major axis cuts.

#### 4. Fitting Characteristics

The basic result of the profile decomposition process is that 620 of the 659 profiles were successfully fitted with the chosen fitting functions. In this section, we will discuss some of the characteristics of the profile decomposition and the errors as they appear with this sample of galaxies. Our intent is to provide information regarding the characteristics of the fitting; we will present our analysis regarding the structure of disk galaxies elsewhere.



#### 4.1. Fitting Parameters and Morphology

All galaxies included in this sample have lenticular or spiral RC3 Hubble types; however, 61 of the fits have been made with no disk component, indicating a lack of any appreciable exponential component to their brightness profiles. Visual inspection of these galaxies in the PANBG shows many of them to have what appear to be disks even though the profile shows none (e.g., NGC 1784, NGC 1961, NGC 3370); others are possibly misclassified elliptical galaxies (e.g., NGC 2655, NGC 3998, NGC 5485). The galaxies with no disk component span a range in T-Type from -3 to 9 — the entire range of T-Type included in this sample. Early type galaxies are somewhat more likely to be fitted without a disk than are late types, but the trend is not very strong. There is no significant difference in the fit quality (as measured by the tabulated RMS deviation) between the galaxies without disk fits and the sample as a whole.

A total of 113 galaxies were fitted without a bulge component, and although these galaxies range in T-Type from -2 through 9, they are mostly late type galaxies. This, of course, is consistent with the basic behavior of the Hubble classification scheme where bulges are less prominent in later types. Again, the basic fitting quality is the same for galaxies without bulge fits as with the sample in general.

An investigation of the variation of the median fractional errors with T-Type is summarized in Table 6. This table gives for each range of T-Type the median fractional error of each fitting parameter, as well as the number of galaxies included in each median determination. The errors in  $I_e$ ,  $r_e$ , and  $I_0$  show some slight trends which are in the expected senses, but which are small enough to be of questionable significance. The two bulge parameters seem to have somewhat larger median errors for later types, as would be expected as the bulge contribution to the light distribution decreases. We should also note the work of Andredakis and Sanders (1994), who show that the inner regions of late-type spirals are perhaps better represented by an exponential light distribution than a deVaucouleurs' law. Similarly, the disk central intensity error has larger values at earlier types, when the disk contribution is generally lower.

We also looked at the possibility of a fitting quality dependence on the presence or lack of a bar, and we have found nothing significant. The median RMS residual of the fits on non-barred galaxies (Hubble type in the RC3 contains an "A" explicitly) is about 0.14 magnitudes, for barred galaxies ("B") it is 0.15 magnitudes, for mixed types ("X") 0.16 magnitudes, and for objects with no bar classification given in the RC3 we find a value of 0.14 magnitudes. All of these values are sensibly the same as the median value of 0.15 magnitudes found for the full sample, and there is clearly no trend apparent. Table 7 lists the median fractional error of the individual fitting parameters for each bar class; there are no significant trends in these results. We conclude that bars have no discernable effect on the quality of the fits.

Objects which have been fitted with an inner truncation make up about 25% (156/620) of the sample. Remembering that inner truncations were included only if they improved the *weighted* RMS by at least 10%, this serves to justify our initial decision to use that function with this

large data set. Some of these inner-truncations are probably caused by arms or rings at large galactocentric radii (e.g., NGC 2859, NGC 3368, and NGC 5701) – the arm/ring is bright relative to the local disk and thus mimics an inner-truncation. In these cases, the arm/ring is typically faint (peaks near  $24 V - mag \text{ arcsec}^{-2}$ ), and has a short disk scale length. These galaxies are also generally classified as having an outer ring. These objects are identified in Table 1 with a "C" in the comment column. A more-detailed analysis of the presence of an inner-truncation is left for a later study.

#### 4.2. Fitting Parameters and Inclination

An analysis of the unweighted RMS residuals shows little or no trend in the mean value with inclination. We divided the sample into three inclination ranges based solely on the  $R_{25}$  value listed in the RC3, assuming that this isophote corresponds to a flat, circular disk:  $i \leq 30^\circ$  ( $R_{25} \leq 0.0625$ ),  $30^\circ < i \leq 60^\circ$  ( $0.0625 < R_{25} \leq 0.301$ ), and  $i > 60^\circ$  ( $R_{25} > 0.301$ ). Note that no T-Type dependence was included in this inclination estimate. The resulting mean RMS residuals for the low inclination, medium inclination, and high inclination samples are 0.16, 0.19, and 0.21 magnitudes, respectively. These three values are all much less than one standard deviation from each other, so the trend is statistically meaningless. The median RMS residuals for each inclination sample are 0.15 magnitudes, 0.14 magnitudes, and 0.17 magnitudes for the low, medium, and high inclinations, respectively. We conclude that the sample has no significant inclination dependence on the unweighted RMS residuals of the fits.

The quality of the individual fitting components is investigated by computing the median fractional errors within each inclination range; the mean fractional errors are not useful because of the outliers discussed previously. Table 8 provides the results of this investigation, which shows that there are no indications of any inclination dependencies. In Table 8, the first column lists the parameters, and the next three columns give the median relative errors in each inclination range.

Finally, we check if the rate of occurrence of the inner-truncation has any inclination dependence by computing the rate in each inclination range. The rates are  $28\% \pm 6.5\%$  for the low inclination group,  $28\% \pm 3.3\%$  for the medium inclinations, and  $19\% \pm 3.3\%$  for the high inclination sample. Thus, there is no trend significant at the  $2\sigma$  level.

### 5. Conclusions

We have presented one of the largest, if not the largest, collections of spiral and lenticular galaxy brightness profile bulge-disk decompositions yet completed. Of the 659 brightness profiles in our sample, 620 were fit with the deVaucouleurs law plus inner-truncated exponential disk function, while the remaining 39 profiles could not be so fit. The general quality of the fits is quite high, with about 50% of the fits having an unweighted RMS deviation from the data (including

real structures) of less than 0.15 magnitudes and more than 90% have unweighted RMS residuals of less than 0.35 magnitudes. We find no systematic trends in the fitting quality with either galaxy morphology or inclination. Comparison of our fits with those of Boroson (1981) and Kent (1985) show discrepancies attributable to a number of observational and data reduction factors.

Probably the most interesting result from this process of fitting is simply that we achieved a "success" rate of 620/659 (94%) in our fits, compared to success rates of 75/94 (80%) for Kent (1985; spiral and S0 galaxies only) and 16/26 (62%) for Boroson (1981). While these success rates are statistically similar, we wonder if the small number statistics are the only differences. An analysis of the 19 non-fittable disk galaxy profiles from Kent (1985) shows that we found fits for all ten of those galaxies which were also in our sample. For these 10 objects, the mean inclination is  $41^\circ \pm 18^\circ$ , the median is  $42^\circ$ , and only one galaxy (NGC 5566) has an inclination greater than  $60^\circ$ . Thus, Kent's non-fittable galaxies do not tend to be high inclination objects. Furthermore, the RMS deviations of our fits for these same galaxies are generally small, with a median value of 0.15 magnitudes, the same as for our full sample. The principal difference seems to be that we included the inner-truncated disk (ITD) factor in our fits: seven of these 10 galaxies have ITD's in our fits, often with large  $r_h/r_0$  ratios. It is also possible that Kent's simultaneous fitting of the minor axis profiles made his results more sensitive to deviations from the standard fitting functions. A similar analysis of the 10 non-fittable profiles in Boroson's (1981) sample shows us having fits for the nine which are included in our sample. These nine galaxies are also of relatively low inclination (the largest is about  $58^\circ$ ), and have small RMS deviations in our fits (median value of 0.13 magnitudes). However, our fitted parameters show three objects with bulge only, three with a bulge plus exponential disk, and three with a bulge plus ITD; the case for the inclusion of the ITD is not as strong with this set of profiles. We conclude, however, that the inclusion of the ITD term in our fitting functions has allowed us to fit an additional 10% to 15% more galaxies than we would have fit without the inner-truncation term.

It is also interesting that about 25% of the profiles in our sample are fitted better by an inner-truncated disk function than with a plain exponential. Some of these fits are certainly due to the ITD being fitted to outer rings (as indicated by a "C" in the last column of Table 1), and others may be marginal improvements (remember the requirement for a 10% improvement of the *weighted* RMS to include the inner-truncation term), but clearly a significant fraction of the profiles support the physical reality of the inner-truncation in the light distribution. A quantification of the strength of the inner truncation and the search for the origin of this feature is the subject of a future paper.

Acknowledgements: One of the authors (WEB) has been supported by STScI under contract NAS5-26555 for this work. The authors would like to thank M. Hamabe for making the PANBG brightness profiles available to us for this project. We also wish to thank the anonymous referee for some useful suggestions. Part of the data analysis for this paper used STSDAS, which was developed by the Space Telescope Science Institute under U.S. Government contract NAS5-26555.

### A. Effects of Seeing on the Fitting Results

The fitting procedure described in section 3.1 makes no allowance for the effects of seeing other than to start the fitting at a radius larger than  $3''$  to avoid the most-affected portion of the brightness profile. We describe in this Appendix a set of experiments which were used to derive estimates of the correction factors for the fitted parameters to measure more accurately the true parameters of the bulge light distributions.

There are four factors in the profile acquisition process which can influence the fitting results, all of which occur at distinct stages of the process and which can be assumed to be separable. Seeing smears the galaxy light as it travels through the atmosphere, while Poisson noise occurs during the photographic exposure physics and chemistry. Pixellation broadens sharp features during the digitization of the plate, as well as adding some additional Poisson noise, and smearing by the aperture photometry happens as a result of the profile acquisition from the digitized data. Our experiments were designed to investigate only those processes which broaden sharp features of the galaxy light distribution: seeing, pixellation, and aperture photometry.

The PANBG provides seeing estimates for all plates in their Table 4.1; we assume that "seeing" in this case refers to the FWHM of stellar profiles. The tabulated seeing in the PANBG ranges from  $1''$  to  $7''$  and is included in our Table 1.

We attempted to replicate the profile definition process as accurately as possible utilizing computer-generated images. These images consist of a perfectly circular deVaucouleur's light distribution with input values of  $I_e = 1000$  in arbitrary intensity units and  $r_e = 0.5, 1, 2, 4, 8, 16,$  and  $32''$ . Poisson noise was included in the images. No disk component was included in these images because the most pronounced effects of seeing will be on the bulge component due to its very steep slope at small radii. We generated  $512 \times 512$  pixel images with these characteristics, assuming a pixel scale of  $3 \text{ pixels}/''$  (to simulate the photographic resolution), then smeared them with Gaussians of FWHM=1, 2, 3, 4, 5, 6, and  $7''$  to simulate the effect of the atmosphere during a long exposure. The resulting images were then block averaged with a  $3 \times 3$  pixel ( $1''$  square) block to replicate the plate scanning utilized for most of the galaxies in the PANBG. Finally, the brightness profiles from the simulated images were extracted using a set of variable diameter circular apertures along a single radius of the "galaxies." These profiles were then fitted in the same fashion as the real profiles in order to estimate the functional parameters, using a fixed fitting range of  $3''$  to  $48''$ . A second set of images was generated using the same input parameters, but which were not smeared by the Gaussians; these images were used to determine the correction factors due to the pixellation and profile acquisition aperture photometry prior to estimating the effects of smearing with a Gaussian.

The results of this procedure are presented in Table 9, which includes for each simulation the seeing size in arcseconds, the input  $I_e$  and  $r_e$ , the fitted  $I_e$  and  $r_e$ , and the ratio of each fitted parameter to its input value, all based on the fully-degraded brightness profiles. The  $I_e$  are all in arbitrary intensity units, and the  $r_e$  are all in simulated arcseconds. Figure A1 shows

the relationship between the fitted:input  $I_e$  as a function of the fitted:input  $r_e$ ; the two quantities are highly anti-correlated, suggesting that the fitted parameters are not truly independent of one another.

As can be seen from the table, there are some cases where the fitted parameters are very different from the input values: the worst cases, as would be expected, are where the seeing disk is large compared to the input  $r_e$ . For  $r_e$ , the percent errors range from less than 1% to almost 40% (seeing=7",  $r_e = 1''$ ), while for  $I_e$  the range is from almost 0% (seeing=4",  $r_e = 32''$ ) to more than 1000% (seeing=7",  $r_e = 1''$ ). We have every reason to suspect that similar fitting errors exist in the PANBG fits, and a means of correcting these errors is highly desirable.

The correction procedure has been separated into two stages: first correct the fitted parameters for the combined effects of pixellation and aperture photometry, then correct these modified parameters for the effects of the Gaussian smearing. The pixellation/aperture photometry correction for the effective radius, based on the simulations without Gaussian smearing, has been found to be well-represented by a power law of the form

$$\log(r'_e/r_e) = 0.005\log(b/r_e) - 0.018 \quad (\text{A1})$$

or

$$r'_e = 0.959r_e(b/r_e)^{0.005} \quad (\text{A2})$$

where  $r_e$  is the fitted effective radius,  $b$  is the digitization aperture size (1"), and  $r'_e$  is the effective radius corrected for the effects of pixellation and aperture photometry; the units of all quantities are in arcsec. This function has a correlation coefficient of 0.989, and a maximum percentage error of 0.2% within the parameter space studied.

The pixellation/aperture correction function for the effective intensity is similarly found to be

$$I'_e = [0.068\log(b/r_e) + 1.246]I_e \quad (\text{A3})$$

where  $I_e$  is the fitted effective intensity,  $r_e$  is the fitted effective radius,  $b$  is the digitization aperture size, and  $I'_e$  is the effective intensity corrected for pixellation and aperture photometry. This function has a correlation coefficient of 0.995 and a maximum percentage error of 0.6% within the parameter space studied. Figure A2 shows the fits of the pixellation/aperture photometry correction functions for both  $r_e$  and  $I_e$ .

The seeing correction is applied by the linear interpolation of the galaxy parameters on the model parameters for the same value of seeing. In Table 10 we list the model data used in the interpolation; column 1 lists the seeing in arcsec ( $S$ ), column 2 the ratio of the seeing to the pixellation-corrected effective radius ( $S/r'_e$ ), column 3 the ratio of the input effective intensity

to the pixellation-corrected effective intensity ( $I_e^0/I_e'$ ), and column 4 the ratio of the input effective radius to the pixellation-corrected effective radius ( $r_e^0/r_e'$ ). The interpolation procedure is performed by computing the  $S/r_e'$  ratio for a fit, and interpolating the  $I_e^0/I_e'$  and  $r_e^0/r_e'$  ratios for the tabulated seeing disk size to derive the fully-corrected  $I_e^0$  and  $r_e^0$  from the previously-computed values of  $I_e'$  and  $r_e'$  (eqs. A2 and A3).

We include in Table 1 the corrected bulge parameters resulting from the described correction procedure. Corrections for objects whose fitted parameters lie outside of the interpolation parameter space are not provided in Table 1.

## REFERENCES

- Andredakis, Y.C., Peletier, R.F., and Balcells, M. 1995, MNRAS, 275, 874
- Andreyakis, Y.C. and Sanders, R.H. 1994, MNRAS, 267, 283
- Baggett, W.E., Baggett, S.M., and Anderson, K.S.J. 1993, BAAS, 24, 1223
- Bevington, P.R. 1969, *Data Reduction and Error Analysis for the Physical Sciences*, (McGraw-Hill Book Company, New York), p 184
- Boroson, T. 1981, ApJS, 46, 177
- Burstein, D. 1979, ApJ, 234, 435
- Byun, Y.I., and Freeman, K.C. 1995, ApJ, 448, 563
- deJong, R. 1996, A&A, 313, 45
- Freeman, K.C. 1970, ApJ, 160, 811
- Holmberg, E. 1947, Medd. Lund. Astr. Obs., Ser. 2, No. 120
- Hubble, E. 1930, ApJ, 71, 231
- Kent, S. 1985, ApJS, 59, 115
- King, I.R. 1966, AJ, 71, 64
- Kodaira, K., Okamura, S., and Ichikawa, S. (eds.) 1990, *Photometric Atlas of Northern Bright Galaxies*, (University of Tokyo Press, Tokyo) (PANBG)
- Kormendy, J. 1977, ApJ, 217 406
- Longo, G. and deVaucouleurs, A. 1983, *The University of Texas Monograph in Astronomy*, No. 3, (University of Texas, Austin)
- Sandage, A. 1961, *The Hubble Atlas of Galaxies*, (Carnegie Institution of Washington, Washington)
- Sandage, A. and Tammann, A. 1981, *A Revised Shapley-Ames Catalog of Bright Galaxies*, (Carnegie Institution of Washington, Washington) (RSA)
- deVaucouleurs, G. 1953, MNRAS, 113, 134

deVaucouleurs, G., deVaucouleurs, A., Corwin, H.G., Buta, R.J., Paturel, G., and Fouque, P.  
1991, *Third Reference Catalogue of Bright Galaxies*, (Springer-Verlag, New York)

Fig. 1.— Brightness profile fits to the NGC 3145 data. Both plots show the bulge component, the disk component, and the sum of the two. The horizontal line at  $25.3 V - mag arcsec^{-2}$  indicates the range of radius included in the fit. *Left*: Fit without a truncation term in the disk component; the RMS deviation of this fit is 0.28 mag. *Right*: Fit including the truncation term in the disk component; the RMS deviation of this fit is 0.12 mag.

Fig. 2.— Brightness profile fits to the galaxies presented in Table 1. Each plot shows the observed profile (crosses), the bulge and disk components and their sum (solid lines), and the range of radius included in the fit (horizontal line(s) at bottom). Also shown are the fitted parameters, where the surface brightness parameters are in units of  $V - mag arcsec^{-2}$  and the size parameters are in arcseconds.

Fig. 3.— Distribution of RMS deviations of the fits from the data. The RMS deviations were computed for all data points in each profile between 3 arcsec and the first point at which the surface brightness drops below  $25 V - mag arcsec^{-2}$ . The median value of the distribution is at 0.15 mag. There are six objects which have RMS deviations greater than 1.0 mag which are not included in the figure.

Fig. 4.— Histograms of the fractional errors. The distributions of the estimated fractional errors of each fitted parameter are shown to illustrate the problem with outliers: a)  $I_e$ , b)  $r_e$ , c)  $I_0$ , d)  $r_0$ , and e)  $r_h$ . Note the smaller bin size for  $r_0$  and  $r_h$ .

Fig. 5.— Comparison of fitted parameters. The fit parameters for the galaxies in common with Boroson (1981) (plus signs) and Kent (1985) (asterisks) are shown along with the 45-degree line. The surface brightness parameters are expressed in units of  $mag arcsec^{-2}$  and the length parameters are given in  $arcsec$ . There is a reasonable correlation for all of the parameters, although the disk parameters have tighter correlations than those for the bulge.

Fig. 6.— Relationship between  $I_e$  fitting accuracy and  $r_e$  fitting accuracy. The apparent anticorrelation suggests some dependence of the fitting parameters on each other.

Fig. 7.— Pixellation/aperture photometry correction functions. a) The data and fit for the correction function for  $r_e$  is shown in a log-log plot. There is clearly a systematic residual function, but it is of insignificant amplitude. b) The data and fit for the  $I_e$  correction function is shown; again there is an insignificant systematic residual, particularly at large values of  $b/r_e$ .